ELSEVIER

Journal of Hydrology 270 (2003) 105–134

Journal of Hydrology

www.elsevier.com/locate/jhydrol

A global hydrological model for deriving water availability indicators: model tuning and validation

Petra Döll*, Frank Kaspar, Bernhard Lehner

Center for Environmental Systems Research, University of Kassel, D-34109 Kassel, Germany

Received 4 December 2001; revised 13 August 2002; accepted 30 August 2002

Abstract

Freshwater availability has been recognized as a global issue, and its consistent quantification not only in individual river basins but also at the global scale is required to support the sustainable use of water. The WaterGAP Global Hydrology Model WGHM, which is a submodel of the global water use and availability model WaterGAP 2, computes surface runoff, groundwater recharge and river discharge at a spatial resolution of 0.5°. WGHM is based on the best global data sets currently available, and simulates the reduction of river discharge by human water consumption. In order to obtain a reliable estimate of water availability, it is tuned against observed discharge at 724 gauging stations, which represent 50% of the global land area and 70% of the actively discharging area. For 50% of these stations, the tuning of one model parameter was sufficient to achieve that simulated and observed long-term average discharges agree within 1%. For the rest, however, additional corrections had to be applied to the simulated runoff and discharge values. WGHM not only computes the long-term average water resources of a country or a drainage basin but also water availability indicators that take into account the interannual and seasonal variability of runoff and discharge. The reliability of the modeling results is assessed by comparing observed and simulated discharges at the tuning stations and at selected other stations. The comparison shows that WGHM is able to calculate reliable and meaningful indicators of water availability at a high spatial resolution. In particular, the 90% reliable monthly discharge is simulated well. Therefore, WGHM is suited for application in global assessments related to water security, food security and freshwater ecosystems.

Keywords: Hydrology; Global model; Discharge; Runoff; Water availability; Model tuning

1. Introduction

Generally, freshwater is generated, transported and stored only within separate river basins. Therefore, for most freshwater quantity and quality issues, the river basin is considered to be the appropriate spatial unit for analysis and management. There are some aspects of freshwater, however, that ask for approaches beyond the basin scale, e.g. for global-scale approaches. First, it is the need for international financing of water-related projects in developing countries, which asks for a global-scale analysis method. Here, a global water availability and use model can help to identify present and future problem areas in a consistent manner, by computing water stress indicators and how they might evolve due to

* Corresponding author. Tel.: +49-561-804-3913; fax: +49-561-804-3176.

E-mail address: doell@usf.uni-kassel.de (P. Döll).

00022-1694/03/$ - see front matter © 2002 Elsevier Science B.V. All rights reserved.
PII: S0022-1694(02)00283-4

global change. Another reason for a global modeling approach to freshwater is the truly global issue of anthropogenic climate change. In order to make climate change simulations more reliable, an improved representation of the terrestrial part of the global water cycle and thus of the processes simulated by hydrological models is required. A third important aspect is the so-called 'virtual water', i.e. the water that is used for producing goods that are then traded between river basins or even globally. The production of 1 kg of beef, for example, may require 10 m^3 of water or more if irrigated grains are used as fodder, a volume that is sufficient to fulfill the basic domestic water requirement of a person during more than half a year. Due to global trade patterns, a global modeling approach is necessary to evaluate the effect of virtual water trading on basin-specific water resources. Finally, environmental problems like freshwater scarcity that do occur on a significant fraction of the Earth's land area and are likely to become even more relevant in the future should be considered to be global problems which require a global analysis.

A first global-scale assessment of water resources and their use was performed in the framework of the 1997 United Nations Comprehensive Assessment of the Freshwater Resources of the World (Raskin et al., 1997). This assessment, however, suffered from the lack of a global modeling approach for water availability and use. The smallest spatial units for which water stress indicators could be computed were whole countries, as both water resources and use information was only available for these units. Besides, the important impact of climate variability (both seasonal and interannual) on water stress could not be taken into account. Finally, scenario generation was inflexible; for example, the impact of climate change on future water availability and irrigation requirements could not be assessed.

To overcome the above restrictions and to achieve an improved assessment of the present and future water resources situation, the global model of water availability and water use WaterGAP (**Water**-**G**lobal **A**ssessment and **P**rognosis) was developed (Döll et al., 1999; Alcamo et al., 2000). With a spatial resolution of 0.5° by 0.5°, it simulates the impact of demographic, socioeconomic and technological change on water use as well as the impact of climate change and variability on water availability and irrigation water requirements. It consists of two main parts, the Global Water Use Model and the Global Hydrology Model, which are linked in order to compute water stress indicators and to calculate the reduction of river discharge due to consumptive water use, i.e. the part of the withdrawn water that evapotranspirates during use and thus does not return to the river. The Global Water Use Model comprises sub-models for each of the water use sectors irrigation (Döll and Siebert, 2002), livestock, households and industry (Döll et al., 2001). Irrigation water requirements are modeled as a function of cell-specific irrigated area, crop and climate, and livestock water use is calculated by multiplying livestock numbers by livestock-specific water use. Household and industrial water use in grid cells are computed by downscaling published country values based on population density, urban population and access to safe drinking water.

The aim of this paper is to show and discuss the capability of the newest version of the **W**aterGAP **G**lobal **H**ydrology **M**odel WGHM to derive indicators of water availability. For each of the 0.5° grid cells, WGHM computes time series of monthly runoff (as fast surface/subsurface runoff and groundwater recharge) and river discharge. Runoff is determined by calculating daily water balances of soil and canopy as well as of lakes, wetlands and large reservoirs (vertical water balance). The lateral transport scheme takes into account the storage capacity of groundwater, lakes, wetlands and rivers and routes river discharge through the basin according to a global drainage direction map. In addition, the discharge reduction by consumptive water use is estimated. Due to the complexity of the processes, the large scale and the limited quality of the input data, WGHM (or any other hydrological model) cannot be expected to compute good runoff and discharge estimates by only using independent data sets. Hence, WGHM was tuned against time series of annual river discharges measured at 724 globally distributed stations by adjusting only one model parameter within plausible limits. The tuning goal was to accurately simulate the long-term average discharges. For about half of the tuning basins, however, this goal could only be achieved by additionally correcting the model output (runoff or discharge). In this paper, 'tuning' means both the adjustment of the model parameter and the model output correction (where necessary). Model

tuning does not necessarily improve the dynamical behavior of the Global Hydrology Model or its sensitivity with respect to climate change but might in some cases even make it worse (e.g. in snow-dominated areas where tuning mainly compensate the underestimation of the input variable precipitation). It leads, however, to more realistic absolute values of the water availability indicators, which is important if water availability is to be compared to water use.

Section 2 provides an overview of other global hydrological modeling approaches. In Section 3, WGHM is described together with its input data sets, the tuning and the regionalization of the calibration parameter. Section 4 presents global maps of selected water availability indicators computed by WGHM, while model performance is discussed in Section 5. Finally, conclusions with respect to model capabilities and future model improvements are drawn.

2. Review of global hydrological models

To the authors' knowledge, there are four other global hydrological models with a spatial resolution of 0.5° besides WGHM (Yates, 1997; Klepper and van Drecht, 1998; Arnell, 1999a,b; Vörösmarty et al., 1998). 0.5° is the highest resolution that is currently feasible for global hydrological models as climatic input is not available at a better resolution. All of the above models are driven by monthly climatic variables. The model of Yates (1997) is a simple monthly water balance model, which does not include independent data sets like soil water storage capacity or land cover but derives the necessary input data based on a climate-vegetation classification. The model of Klepper and van Drecht (1998) operates on a daily time step but assumes that precipitation is distributed equally over all days of the month. It is based on a number of independent data sets regarding soil, vegetation and other geographical information. In particular, it contains a heuristic algorithm to partition total runoff into surface runoff and groundwater recharge which has been modified and extended for WGHM. For some of the compared large river basins, these two models represent the spatially and temporally averaged runoff regime quite well. However, lateral routing is not taken into account in either model (nor in the model of Arnell, 1999a,b), which prevents a correct runoff computation where wetlands are fed by lateral inflow.

The hydrological models Macro-PDM of Arnell (1999a, b), WBM of Vörösmarty et al. (1998) and WGHM (this paper) try to simulate the actual soil moisture dynamics by generating pseudo-daily precipitation from information on monthly precipitation and the number of wet days in each month. All three use a simple degree-day algorithm to simulate snow, and they allow runoff generation to occur even if the soil moisture store is not completely filled. Unlike WBM, WGHM and Macro-PDM explicitly simulate interception. In an application to Europe, Arnell (1999a) tuned some Macro-PDM model parameters uniformly across the continent but did not perform a basin-specific calibration. As a result, a difference of 50% ore more between simulated and observed long-term average runoff in large European river basins was not uncommon. Meigh et al. (1999) applied a different version of Macro-PDM for a water resources assessment in Eastern and Southern Africa. Here, runoff was routed laterally with a monthly time step, taking into account the storage of lakes, reservoirs and wetlands as well as the reduction of river discharge due to evaporation, river channel losses and human water consumption. Meigh et al. did not calibrate the vertical water balance but adjusted some other parameters in a basin-specific manner, in particular artificial transfers between cells and the river channel loss coefficients. A comparison of annual and monthly discharge values for 96 drainage basins with areas in the range between 7 km^2 and more than 1,000,000 km^2 showed that even in many large basins the simulated long-term average discharges differed by more than 50% from the observed values.

Fekete et al. (1999) applied the macro-scale hydrological model WBM of Vörösmarty et al. (1998) at the global scale to derive long-term average runoff fields. They combined the information from discharge measurements at 663 stations with model results not by calibration (i.e. by adjusting some model parameters) but by the introduction of a correction factor that is equal to the ratio of measured and simulated long-term average discharge. Thus, Fekete et al. used the hydrological model WBM for a spatial interpolation of the observed long-term average runoff in basins with

discharge measurements, while elsewhere they calculated runoff with the standard model parameterization of WBM. However, the computed long-term average runoff distribution is not consistent due to the following two reasons:

- The time period of the applied long-term average climatic variables mostly does not coincide with the many different time periods of the measured long-term average discharges
- Reduction of river discharge by human water consumption was not considered. Therefore, runoff is underestimated in basins with significant consumption.

Global runoff computations are also performed by all global climate models, but it is generally accepted that these estimates are poor. Their modeling algorithms are not well suited to represent the soil water processes, their spatial resolution is very low and they are not calibrated against measured discharge. Oki et al. (1999) compared the discharge computed by 11 land surface models in an offline mode for 1987/88 to discharge observations at 250 stations in 150 large river basins (after routing along a 1° by 1° global drainage direction network). They found that the error increased significantly if rain gauge density was below 30 per 10^6 km^2. The computed discharges at a certain station varied strongly with the land surface model. For example, for the Mississippi at Vicksburg (drainage basin area 2,960,000 km^2), the range of the computed values was 24 to 130 mm/yr, while the observed value was 142 mm/yr.

Nijssen et al. (2001) used an extended version of the VIC model of Liang et al. (1994) to model runoff and discharge at the global scale. The VIC model, which was designed to be a land surface module for climate models, was applied at a spatial resolution of 2° by 2° and with daily climatic input (time series 1979–1993). Lateral routing was performed at a 1° resolution. The model was calibrated against discharge time series observed at 22 globally distributed stations by adjusting four parameters specifically for each basin and two parameters according to the climatic zone. The six parameters were then regionalized to the non-calibrated grid cells according to the climate zone. After calibration, the computed 1980–1993 average annual discharge differed on average by 12% from the observed value (0.9–22%, excluding the Senegal with 340%), and the mean monthly hydrographs showed fairly strong discrepancies between observed and computed values. For example, the differences between the monthly flow volumes during the low and high flow seasons of the Congo, Danube, Parana and Mississippi were strongly overestimated.

This review of global hydrological models shows that it is necessary to use information from discharge measurements to obtain reasonable estimates of runoff and discharge at the global scale. Unfortunately, it currently appears to be impossible to achieve a good agreement of model results with measured discharge values without applying, at least for a significant number of river basins worldwide, a correction factor to the modeled values. Such a correction factor is applied both by Fekete et al. (1999) to WBM and by us to WGHM (see Section 3.6) to achieve that the long-term average discharges are represented reasonably well. The disadvantage of this approach is that in these basins runoff and discharge (after correction) are no longer consistent with computed evapotranspiration or soil water content.

3. Model description

3.1. Spatial base data

The computational grid of WaterGAP 2 consists of 66896 cells of size 0.5° geographical latitude by 0.5° geographical longitude and covers the global land area with the exception of Antarctica. It is based on the 5′ land mask of the FAO Soil Map of the World (FAO, 1995). A 0.5° cell that contains at least one 5′ land cell is defined as a computational cell. For each 0.5° cell, information on the fraction of land area and of freshwater area is available. The latter information is derived from a compilation of geographic information on lakes, reservoirs and wetlands at a resolution of 1′ (Lehner and Döll, 2001, see Section 3.3.1).

The upstream/downstream relation among the grid cells, i.e. the drainage topology, is defined by the new global drainage direction map DDM30, which represents the drainage directions of surface water at

a spatial resolution of 0.5° (Döll and Lehner, 2002). Each cell either drains into one of its eight neighboring cells or represents an inland sink or a basin outlet to the ocean. Based on DDM30, the drainage basin of each cell can be determined. A validation against independent data on drainage basin area showed that DDM30 provides a more accurate representation of drainage directions and river network topology than other 30′ DDMs (Döll and Lehner, 2002).

3.2. Climate input

The global data set of observed climate variables by New et al. (2000) provides climate input to WaterGAP 2. It comprises monthly values of precipitation, temperature, number of wet days per month, cloudiness and average daily sunshine hours (and other variables), interpolated to a 0.5° by 0.5° grid for the complete time series between 1901 and 1995 (except for sunshine, where only the long-term average values of the period 1961–1990 are given).

In WaterGAP 2, calculations are performed with a temporal resolution of one day. Synthetic daily precipitation values are generated from the monthly values by using the information on the number of wet days per month. The distribution of wet days within a month is modeled as a two-state, first-order Markov chain, the parameters of which were chosen according to Geng et al. (1986). The total monthly precipitation is distributed equally over all wet days of the month.

Daily potential evapotranspiration E_{pot} is computed according to Priestley and Taylor (1972). Following the recommendation of Shuttleworth (1993), the α-coefficient is set to 1.26 in areas with an average relative humidity of 60% or more and to 1.74 in other areas. Net radiation is computed as a function of the day of the year, latitude, sunshine hours and short-wave albedo according to Shuttleworth (1993), except for the computation of the sunset hour angle which we believe to be better approximated by the CBM model of Forsythe et al. (1995). The computed net radiation and thus the potential evapotranspiration are very sensitive to the use of either the sunshine hours, the cloudiness or the global radiation data set as provided by New et al. (2000). The resulting potential evapotranspiration appears to be too low unless the sunshine hours data set is used. Therefore, a time series of mean monthly sunshine hours is generated from the long-term averages as provided by New et al. (2000) by scaling them with the cloudiness time series. Daily values of sunshine hours as well as of temperature are derived from the monthly values by applying cubic splines.

3.3. Vertical water balance

Within each grid cell, the vertical water balances for open water bodies (lakes, reservoirs and wetlands) and for the land area are computed separately. Fig. 1 provides a schematic representation of how the vertical water balance and the lateral transport are modeled in WGHM.

3.3.1. Vertical water balance of freshwater bodies

A representation of open inland waters (wetlands, lakes and reservoirs) is important for both the vertical water balance, due to their high evaporation, and for the lateral transport, due to their retention capacity. A new global data set of wetlands, lakes and reservoirs was generated (Lehner and Döll, 2001), which is based on digital maps (ESRI, 1993—wetlands, lakes and reservoirs; ESRI, 1992—wetlands, lakes, reservoirs and rivers; WCMC, 1999—lakes and wetlands; Vörösmarty et al., 1997—reservoirs) and attribute data (ICOLD, 1998—reservoirs; Birkett and Mason, 1995—lakes and reservoirs). Wetlands also encompass some stretches of large rivers, i.e. the floodplains. The data set distinguishes local from global lakes and wetlands, the local open water bodies being those that are only reached by the runoff generated within the cell and not by discharge from the upstream cells. The data set contains the areas and locations of 1648 lakes larger than 100 km^2 and of 680 reservoirs with a storage capacity of more than 0.5 km^3. In addition, some 300,000 smaller ‘lakes’ are taken into account, for which it could not be determined whether they are natural lakes or man-made reservoirs. In the data set, wetlands cover 6.6% of the global land area (not considering Antarctica and Greenland), and lakes and reservoirs 2.1%.

In WGHM, actual evaporation from open water bodies is assumed to be equal to potential evapotranspiration, and runoff is the difference between precipitation and potential evapotranspiration. The freezing of open water bodies is not considered, and precipitation is always assumed to become liquid as

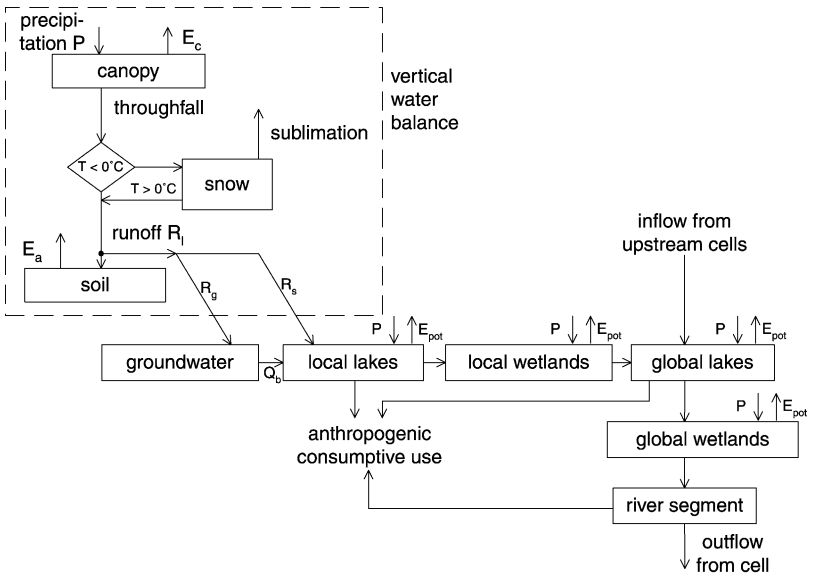

Fig. 1. Schematic representation of the global hydrological model WGHM, a module of WaterGAP 2 (E_{pot}: potential evapotranspiration, E_a: actual evapotranspiration from soil, E_c: evaporation from canopy). The vertical water balance of the land and open water fraction of each cell is coupled to a lateral transport scheme, which first routes the runoff through a series of storages within the cell and then transfers the resulting cell outflow to the downstream cell. The water volume corresponding to human consumptive water use is taken either from the lakes (if there are lakes in the cell) or the river segment.

soon as it reaches the water body. Potential evapotranspiration is assumed to be the same for all types of open water bodies and land areas. In reality, wetland evapotranspiration can either be lower or higher than open water evaporation, but not enough information exists to model different evaporative behaviors. In WGHM, the main difference between lakes (and reservoirs) and wetlands is that the latter can dry out, while the former are assumed to have a constant surface area from which evaporation occurs. However, the gradual changes of wetland extent during desiccation are not modeled. It is assumed that as long as water is stored in the wetland, its area is constant.

3.3.2. Vertical water balance of land areas (canopy and soil water balances)

The vertical water balance of land areas is described by a canopy water balance (representing interception) and a soil water balance (Fig. 1). The canopy water balance determines which part of the precipitation evaporates from the canopy, and which part reaches the soil. The soil water balance partitions the incoming throughfall into actual evapotranspiration and total runoff. Finally, the total runoff from the land area is partitioned into fast surface runoff and groundwater recharge.

The effect of snow is simulated by a simple degree-day algorithm. Below 0 °C, precipitation falls as snow and is added to snow storage. Above 0°, snow melts with a rate of 2 mm/d per degree in forests and of 4 mm/d in the case of other land cover types. Land cover of the land areas is assumed to be homogeneous within each grid cell. The global 0.5° land cover grid as modeled by IMAGE 2.1 (Alcamo et al., 1998), which distinguishes 16 classes, is used for WGHM.

Canopy water balance. Canopy storage enables evaporation of intercepted precipitation before it reaches the soil. In case of a dry soil, for example, interception generally leads to increased total evapotranspiration. Interception is simulated by computing the balance of the water stored by the canopy as a function of total precipitation, throughfall and canopy evaporation. Following Deardorff (1978), canopy evaporation E_c [mm/d] is described as

$$E_c = E_{pot}\left(\frac{S_c}{S_{cmax}}\right)^{2/3} \quad (1)$$

with $S_{cmax} = 0.3$ mm LAI

where S_c = water stored in the canopy [mm], S_{cmax} = maximum amount of water that can be stored in the canopy [mm] and LAI = one-sided leaf area index. Daily values of the leaf area index are modeled as a function of land cover, leaf mass (as provided by the IMAGE 2.1 model of Alcamo et al., 1998) and daily climate. LAI is highest during the growing season, i.e. when temperature is above 5 °C and the monthly precipitation is more than half the monthly potential evapotranspiration. No difference is made between the interception of rain and snow.

Soil water balance. The soil water balance takes into account the water content of the soil within the effective root zone, the effective precipitation (the sum of throughfall and snowmelt), the actual evapotranspiration and the runoff from the land surface. The soil is modeled as one layer. Capillary rise from the groundwater cannot be taken into account as no information on the position of the groundwater table is available at the global scale.

Actual evapotranspiration from the soil E_a [mm/d] is computed as a function of potential evapotranspiration from the soil (the difference between the total potential evapotranspiration and the canopy evaporation), the actual soil water content in the effective root zone and the total available soil water capacity as

$$E_a = \min\left((E_{pot} - E_c), (E_{potmax} - E_c)\frac{S_s}{S_{smax}}\right) \quad (2)$$

where E_{potmax} = maximum potential evapotranspiration [mm/d] (set to 10 mm/d), S_s = soil water content within the effective root zone [mm], S_{smax} = total available soil water capacity within the effective root zone [mm]. The smaller the potential evapotranspiration from the soil, the smaller is the critical value of S_s/S_{smax} above which actual evapotranspiration equals potential evapotranspiration. S_{smax} is computed as the product of the total available water capacity in the uppermost meter of soil (Batjes, 1996) and the land-cover-specific rooting depth.

Following the approach of Bergström (1995), total runoff from land R_l [mm/d] is computed as

$$R_l = P_{eff}\left(\frac{S_s}{S_{smax}}\right)^{\gamma} \quad (3)$$

where P_{eff} = effective precipitation [mm/d], γ = runoff coefficient (calibration parameter).

The daily balance of throughfall and snowmelt on the one hand and E_a and R_l on the other hand leads to a changing soil moisture content S_s. In the next time step this affects E_a and R_l as both are computed as a function of S_s. Thus the runoff coefficient γ is also directly affecting E_a.

Applying a heuristic approach, total runoff from land is partitioned into fast surface and subsurface runoff and groundwater recharge using globally available data on slope characteristics within the cell (Günther Fischer, IIASA, Laxenburg, Austria, personal communication, 1999), soil texture (FAO, 1995), hydrogeology (Canadian Geological Survey, 1995) and the occurrence of permafrost and glaciers (Brown et al., 1998; Hölzle and Häberli, 1999). For each cell, daily groundwater recharge R_g is computed as

$$R_g = \min(R_{gmax}, f_g R_l) \quad (4)$$

with $f_g = f_s f_t f_a f_{pg}$ where R_{gmax} = soil texture specific maximum groundwater recharge [mm/d], f_g = groundwater recharge factor, f_s = slope-related factor, f_t = texture-related factor, f_a = aquifer-related factor, f_{pg} = permafrost/glacier-related factor. A detailed description of groundwater recharge modeling is given in Döll et al. (2000).

3.4. Lateral transport

Within each grid cell, the runoff produced inside the cell and the inflow from the upstream cell(s) are transported through a series of storages which represent the groundwater, lakes, reservoirs, wetlands and the river (Fig. 1). The resulting cell outflow then becomes the inflow of the downstream cell.

While it is assumed that fast surface/subsurface runoff $R_s(= R_l - R_g)$ is routed to surface storages without delay, groundwater recharge R_g is stored in the groundwater store S_g. Baseflow Q_b is produced in proportion to the stored groundwater as

$$Q_b = -k_b S_g \quad (5)$$

where k_b = baseflow coefficient [1/d]. The baseflow coefficient is set to 0.01/d globally. Note that transport between cells is assumed to occur only as surface water flows and not as groundwater flows, i.e. the complete groundwater recharge of a cell is assumed to

discharge into the surface water (river, lake, wetland) of the same cell. This assumption is necessary as no information on groundwater flow paths is available at the global scale.

Fast surface and subsurface runoff and baseflow then recharge local lakes first if these are present in the cell (Fig. 1). The principal effect of a lake on lateral transport is to reduce the variability of flows, which can be simulated by computing lake outflow Q_{out} as

$$Q_{out} = k_r S_r \left(\frac{S_r}{S_{rmax}} \right)^{1.5} \quad (6)$$

with $S_{rmax} = A_{lake} H$ where k_r = outflow coefficient [1/d] (0.01/d), S_r actual active storage [m^3], S_{rmax} = maximum active storage capacity [m^3], A_{lake} = area of the lake [m^2] and H = maximum active storage depth [m]. The exponent 1.5 is based on the theoretical value of outflow over a rectangular weir (Meigh et al., 1999). The maximum active storage depth is set to 5 m. The behavior of the next storage (Fig. 1), the local wetlands, is modeled similar to Eq. (6), only with a maximum storage depth of 2 m and an exponent of 2.5 instead of 1.5. The lower active storage depth leads to a lower storage capacity of wetlands as compared to lakes, and the higher exponent to a slower outflow. Obviously, the above parameter setting is very arbitrary. In our calculations we found, however, that the 5 m active lake depth gets very rarely used. More investigation are needed to check and improve the simulation of lake and wetland dynamics.

The storage behavior of global lakes and wetlands, the next two consecutive storages (Fig. 1) is simulated like the behavior of their local counterparts. In the current version of WaterGAP 2, reservoirs are treated like global lakes, due to lack of information on their management. In the next transport step, the discharge reaches the river which itself is treated as a linear storage element, similar to the groundwater (Eq. (5)). The outflow coefficient is chosen such that the river water is transported with a velocity of 1 m/s. Finally, the resulting cell discharge becomes the inflow to the next downstream cell.

3.5. Subtraction of consumptive water use

River discharge is affected by water withdrawals and return flows. In basins with extensive irrigation, in particular, discharge is significantly reduced by water use. Using both the water use and water availability values as computed by WaterGAP 2, Kaspar et al. (2001) calculated that in the Colorado (USA), Guadalquivir (Spain) and Indus (Pakistan) basins, for example, consumptive use in 1995 amounts to more than 70% of the natural discharge (long-term 1961–1990 average). In the Chinese Huanghe basin, 30% of the natural discharge is consumed and in the European basins Thames and Danube 20% and 9%, respectively. In the large basins of Central Europe, the value is between 3 and 6%. Therefore, it is imperative to consider the effect of water use in the simulation of discharge.

In the WGHM model, natural cell discharge (without human water use) is reduced, with a daily time step, by the consumptive water use in a grid cell as calculated by the Global Water Use Model of WaterGAP 2 (if enough water is available). The time series of irrigation water use within the simulation period is calculated by taking into account the climate as well as the country's estimated irrigated area of the respective years. Water use for households, industry and livestock is approximated by scaling water use in 1995 based on the population development of each country. If a lake is present in the grid cell, consumptive use can be taken from the lake unless the actual active storage S_r equals zero (Fig. 1). Without lakes, consumptive water use at a certain day can only be subtracted if consumptive use is smaller than river discharge. In many instances, however, it is larger, which may be due to withdrawals from groundwater or from surface water reservoirs not included in WGHM. To account for this, the subtraction of consumptive use can be delayed for up to one year until a period with a discharge surplus occurs (Kaspar et al., 2001). If the annual average of consumptive water use in a cell is larger than the annual average of discharge, an attempt is made to cover the demand for water from the neighboring cell with the highest 1961–1990 long-term average discharge. Even with this modeling approach, a significant part of the computed water demand cannot be covered in many regions of the globe, e.g. the Great Plains of the USA, the Arabian Peninsula and Northern China. This is at least partly due the use of fossil groundwater.

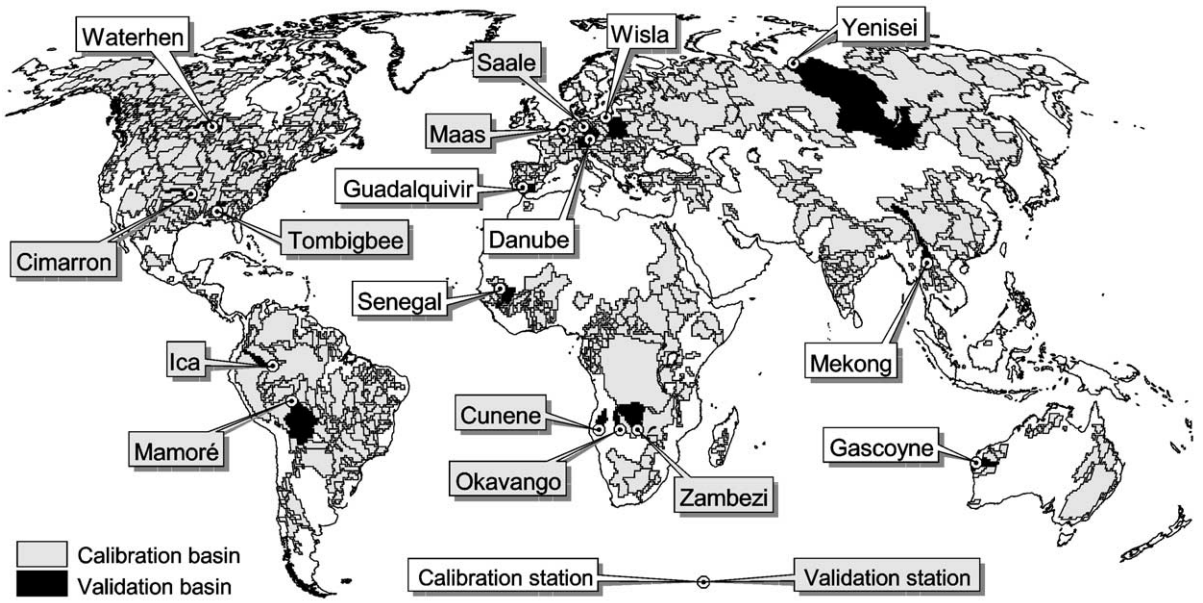

Fig. 2. Location of tuning basins and selected discharge gauging stations (tuning and validation stations referred to in Tables 3 and 4 and Figs. 10–13).

3.6. Model tuning

It is unlikely that a large-scale hydrological model can simulate actual runoff and discharge satisfactorily if it is not adjusted in a basin-specific manner based on observed discharge. The main reasons for this are:

- erroneous input data (precipitation, in particular, as well as radiation)
- sub-grid spatial heterogeneity
- uncertainty with respect to model algorithms (e.g. computation of potential evapotranspiration or discharge reduction by water use)
- neglect of important processes like surface water-groundwater interaction (river losses, capillary rise), the formation of small ponding after short lateral transport and artificial transfers.

Observed discharge provides additional information, and tuning against these measurement values can therefore improve model performance. In order to avoid overparameterization and to enable model tuning in a large number of basins, only the vertical water balance for the land area is tuned by adjusting one model parameter, the runoff coefficient γ (compare Eq. (3)). The goal of our tuning process is to ensure that the long-term average discharges are well represented by the model as they typically form the basis for water stress indicators (Alcamo et al., 2000; Raskin et al., 1997). WGHM has been tuned for 724 drainage basins worldwide (Fig. 2), based on observed discharges provided by GRDC (Global Runoff Data Centre) (1999) Koblenz, Germany, in 1999. The minimum drainage basin size considered is 9000 km^2, and the stations along a river were selected such that the inter-station areas are generally larger than 20,000 km^2. The model is tuned to discharge of the last thirty measurement years (or fewer years, depending on data availability). The tuning basins cover about 50% of the global land area (not considering Greenland and Antarctica) and about 70% of the actively discharging area (Fekete et al., 1999).

In the tuning process, the runoff coefficient of all cells within each individual basin is adjusted homogeneously such that the simulated long-term average discharge at the tuning stations is within 1% of the observed one. The runoff coefficient is allowed to vary only in the range between 0.3 and 3. With a γ below 0.3, considerable runoff will be produced even if the soil is very dry, while with a γ above 3, runoff will be

extremely small even well above the wilting point (compare Eq. (3)). Thus, a runoff coefficient outside the range of 0.3–3 would prevent the hydrological model from simulating the soil water dynamics in a realistic manner. However, even tuning of the soil water balance within plausible limits can, under certain circumstances, lead to an unrealistic simulation of the soil dynamics as it tries to compensate for input data errors, spatial heterogeneity and model formulation errors (see above).

If discharge is underestimated even with a γ of 0.3, or overestimated even with a γ of 3, we suspect that processes have a strong impact which are not taken into account by WGHM (e.g. leakage through river beds) or that input data, in particular precipitation, are significantly inaccurate. In these cases, a runoff correction factor is assigned to each cell within the basin (same value for each cell), to enforce that the simulated and observed long-term average discharges at the basin outlet are within 1%. This runoff correction, however, is complicated by the fact that some of the cells in a basin may have a negative total cell runoff. Negative values are due to global lakes and wetlands in which evaporation of water supplied from upstream is larger than precipitation. If, for example, the computed discharge is smaller than the observed one even with a γ of 0.3, total cell runoff in each cell of the basin is increased by adding the same percentage of its absolute value. In order to prevent a sign change of runoff, i.e. that the runoff from land becomes negative or the runoff from open water surface switches from negative to positive, a maximum change of 100% is allowed. In basins where such a runoff correction factor has to be applied, the model does not correctly simulate the dynamics of the water cycle but only serves to interpolate measured discharge in space and time.

In some basins, the correction of the cell runoff within the tuning basin still does not lead to an agreement between observed and measured discharge. In this case, a second correction is applied directly to the discharge at the measurement station. This discharge correction is done to achieve that the simulated inflow to the downstream drainage basin is similar to the observed values, and leads to a stepwise increase or decrease of discharge from the cell upstream of the measurement cell to the measurement cell itself. The simulated runoff field is not modified by this discharge correction.

In only 385 out of the 724 tuning basins, the long-term average simulated discharge is computed to be within 1% of the observed discharge by applying a runoff coefficient γ that is within the physically plausible range of 0.3–3 (Fig. 3). These basins cover 30.3 million km^2, or 46% of the total area of the tuning basins. In 201 basins, discharge is underestimated even with a γ of 0.3 (24.2 million km^2, or 36% of the calibrated area) if no runoff or discharge correction is applied. These basins are mostly snow-dominated, and the underestimation of discharge can be explained by the fact that snow precipitation is strongly underestimated by precipitation gauges. In some basins, observed runoff is even larger than observed precipitation. Such an underestimation of discharge in snow-dominated basins was also reported by Fekete et al. (1999) and Oki et al. (1999). To test the hypothesis of a precipitation underestimation in snow-dominated basins, the (uncorrected) precipitation values of New et al. (2000) were corrected by applying the monthly precipitation correction factors of Legates and Willmott (1990). Then, discharge in many snow-dominated river basins could be modeled with a runoff coefficient above 0.3. However, simulated discharge in many other basins became too high, and it appears that for example in Central Europe the precipitation correction factors are too high. As no other global precipitation correction data set is currently available, we decided to use uncorrected precipitation.

In 138 out of the 724 tuning basins, discharge would be overestimated, without correction, even with a γ of 3. These basins cover 12.0 million km^2 or 18% of the calibrated area (Fig. 3) and are often located in arid and semi-arid areas. The global hydrological models of Fekete et al. (1999) and Nijssen et al. (2001) also tend to overestimate discharge in the dry regions of the globe. In these regions, the model formulation of WGHM is likely to be incomplete. For example, losses from the river channel to groundwater and/or phreatophyte evapotranspiration, or the evaporation from many small ephemeral ponds forming after rainfall are not taken into account. These processes are likely to be relevant, e.g. in the Nile, the Niger, the Senegal and the Oranje basins. In addition, the evaporation from lakes and wetlands, which is not adjusted by the tuning, may have a larger impact on runoff than the vertical water balance of the land fraction of the basin.

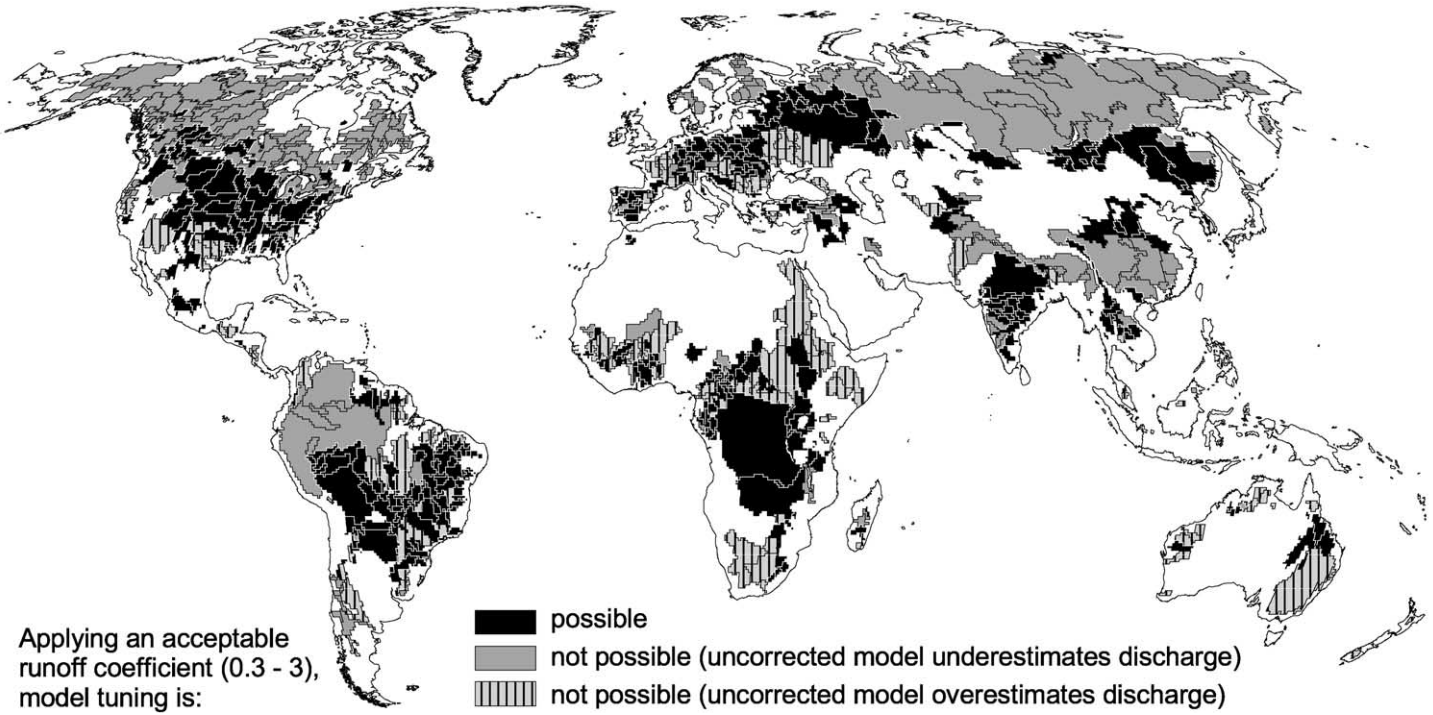

Fig. 3. River basins in which WGHM can be tuned by adjusting the runoff coefficient within plausible limits (0.3–3).

In river basins with large consumptive water use, a relatively small underestimation of subtracted consumptive use might lead to an overestimation of discharge (e.g. Murray-Darling in Australia, lower stretches of the Danube in Romania and Bulgaria). In addition, in some basins river flow is affected by interbasin transfers, a process that is not simulated in WGHM. In the case of the lower Colorado, about 30% of the discharge is exported to adjoining water-scarce basins (Smedena, 2000). The relatively small overestimation of discharge in the French rivers Seine, Loire and Rhone is possibly related to interbasin transfers, too.

In 103 out of the 339 tuning basins in which cell runoff is corrected an additional discharge correction factor had to be introduced. Discharge was corrected downwards in 43 basins (6.4 million km^2), e.g. in basins where river discharge decreases in the downstream direction (e.g. Orange, Colorado). An upward correction was needed in 60 mainly snow-dominated basins (5.7 million km^2), e.g. in many Canadian basins as well as in the Brahmaputra and the Irrawady basins, where observed precipitation is underestimated due to the insufficiently dense precipitation station network (Nijssen et al., 2001).

3.7. Regionalization

Runoff coefficients in the untuned river basins were estimated using a multiple linear regression approach that included tuning basins with the following characteristics:

- The basin is the most upstream sub-basin of the river basin. This ensures that its tuning has not been influenced by the tuning in upstream basins.
- The basin area is at least 20,000 km^2.
- If the runoff coefficient of the tuning basin is 0.3, the 1961–1990 long-term average annual temperature of the basin is below 10 °C. (This includes a large number of snow-dominated basins but excludes a few tropical basins for which we do not see a consistent explanation of their low γ-value).

The runoff coefficients γ of the selected 311 tuning basins were found to be correlated to three basin-specific variables (in decreasing order of predictive capability):

1. 1961–1990 long-term average temperature T_a of the basin,
2. area of open freshwater (with wetlands at their maximum extent) in percent of the total basin area A_{of}
3. the length of non-perennial river stretches within each basin L_{np} (derived from the Digital Chart of the World, ESRI, 1993).

The three variables were tested to be not intercorrelated. A corrected R^2 of 0.53 was obtained with respect to the regression equation

$$\ln \gamma = -0.5530 + 0.0466 T_a - 0.0143 A_{of} + 0.0817 \ln L_{np} \quad (7)$$

Everything else being equal, the smaller the runoff coefficient is, the higher the runoff becomes. Eq. (7) reflects that the runoff coefficient is mostly small in cold, snow-dominated basins and high in warm, dry regions. Eq. (7) was used to compute the runoff coefficients of the regionalized basins, but values were constrained to the range of 0.3–3. Correction factors were not regionalized, i.e. correction factors were set to 1 for all regionalized basins, which may lead to an underestimation of runoff in regionalized basins with $\gamma = 0.3$ and to an overestimation in basins with $\gamma = 3$. Fig. 4 shows the global distribution of tuned and regionalized runoff coefficients. The zonal structure of the regionalized runoff coefficients reflects the dominant regression factor temperature. Consistent with the tuning basins, snow-dominated regionalized basins, e.g. in the Arctic and the Himalayas, are assigned a value of 0.3, while the regionalized γ of most warm regions of the globe is between 1 and 2. Values above 2 are only reached in arid regions.

4. Results

The global distribution of total cell runoff (computed from the vertical water balance for both freshwater bodies and land areas) for the time period 1961–1990 is presented in Fig. 5. As explained above, negative values are due to cells with global lakes and wetlands in which evaporation of water supplied from upstream is larger than precipitation. Please note that in many snow-dominated regions, runoff is likely to be

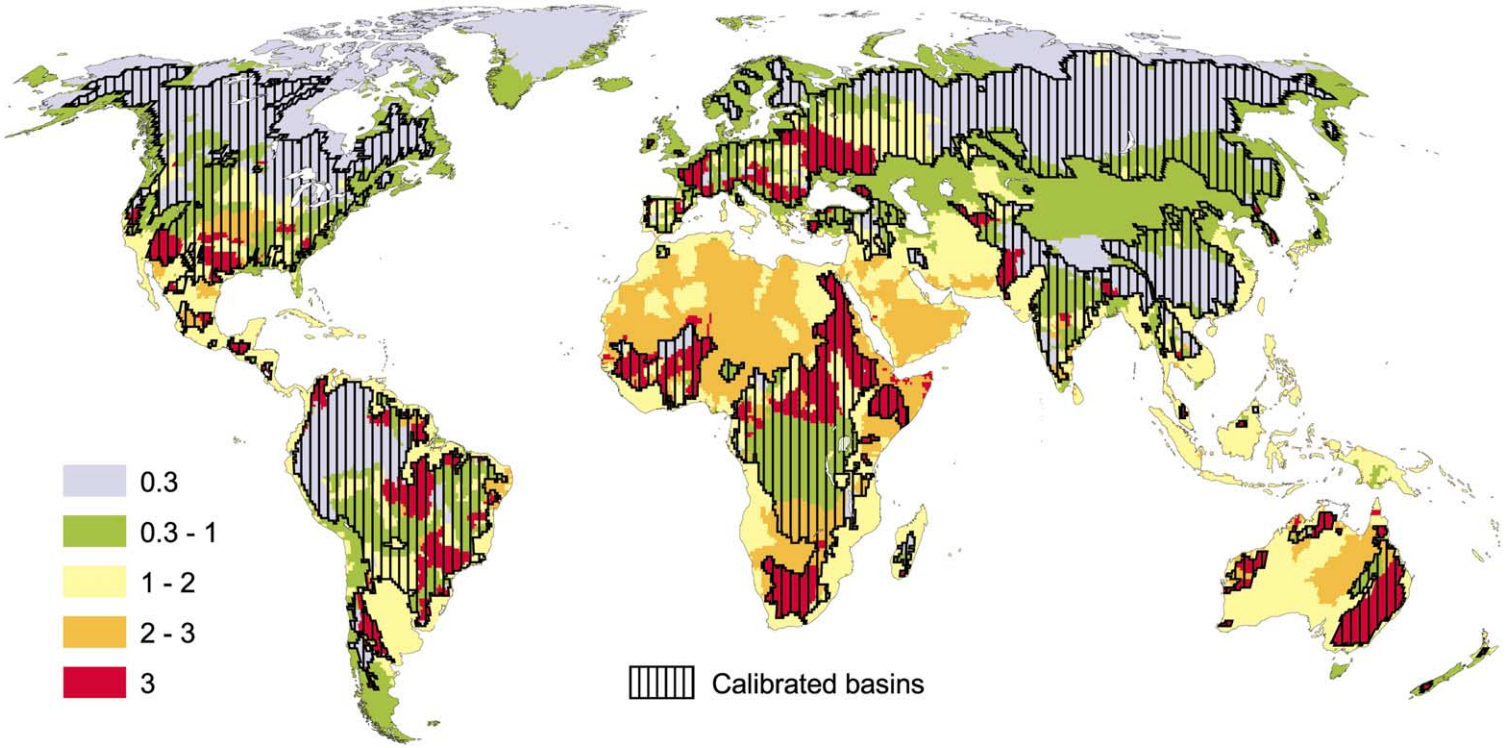

Fig. 4. Runoff coefficients obtained by tuning to measured discharge and by regionalization to river basins without measured discharge.

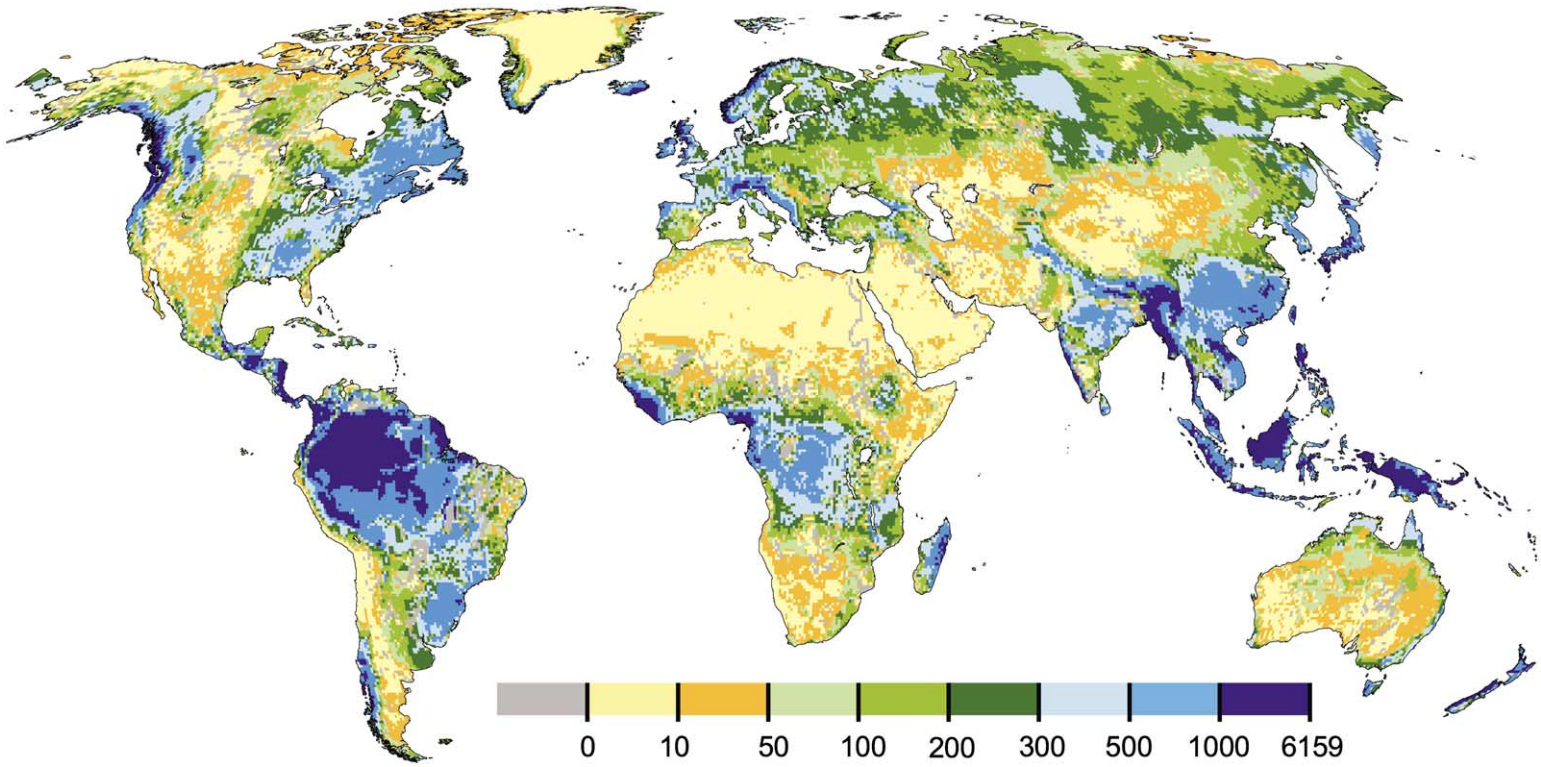

Fig. 5. Long-term average annual total runoff from land and open water fraction of cell (time period 1961–1990), in mm/yr. Negative values are due to the evapotranspiration from open water.

Table 1
Comparison of estimated long-term average continental discharge into oceans and inland sinks, in km^3/yr

Continent	WaterGAP 2[a]		Nijssen et al. (2001, Table 4)[b]	WRI (World Resources Institute) (2000)[c]	Fekete et al. (1999, Table 4)[c]	Korzun et al. (1978, Table 157)[c]	Baumgartner and Reichel (1975, Table 12)[c]
Europe[d]	2763	*936*	n.a.	n.a.	2673	2970	2800
Asia[d]	11234	*2052*	n.a.	n.a.	n.a.	14100	12200
Africa	3529	*1200*	3615	4040	4474	4600	3400
North and Central America[e]	5540	*1980*	6223	7770	6478	8180	5900
South America	11382	*4668*	10180	12030	11708	12200	11100
Oceania[f]	2239	*924*	1712	2400	n.a.	2510	2400
Total land area (except Antarctica)	36687	*11760*	36006	42650	39476	44290	37700

In the case of the WaterGAP 2 estimates, the values in italics are an estimate of long-term average water availability based on the 90% reliable monthly discharge Q_{90}. n.a.: estimate not available for chosen definition of continental extent.

[a] Average 1961–1990.

[b] Average 1980–1993, computed by multiplying runoff with continental areas of WaterGAP 2.

[c] Time period not specified

[d] Eurasia is subdivided into Europe and Asia along the Ural; Turkey is assigned to Asia.

[e] Includes Greenland

[f] Includes the whole island of New Guinea

underestimated, namely in those tuned areas where a discharge correction was necessary (compare Section 3.6) as well as in those areas for which no discharge measurements were available as the runoff correction factor was not regionalized. For tuned semi-arid and arid areas, WGHM possibly tends to underestimate runoff generation as WGHM does not capture some of the complex processes that affect the transfer of runoff to observable river discharge (e.g. leakage from river channels). In basins without discharge measurement, the accuracy of the modeled runoff is unknown; in central Australia, however, the model obviously overestimates runoff.

By accumulating the discharges into the oceans and to inner-continental sinks (e.g. Lake Chad), continental and global water resources are estimated, and can be compared to previous estimates (Table 1). For the computation of continental water resources we use the natural discharge as if no discharge reduction would occur due to human water use. According to the Global Water Use Model of WaterGAP 2, global consumptive water use was 1250 km^3/yr in 1995 (assuming 1961–1990 long-term average climate for the computation of irrigation water use). Therefore, our estimates should be above those of the other authors who directly used observed discharge to obtain their runoff estimates, without taking into account discharge reduction by water use. However, WGHM results in the second lowest value of global water resources. In the case of Europe, Asia, and North and Central America, our estimates might actually be somewhat too low as in these areas precipitation is likely to be underestimated, and the effect of this underestimation on discharge is only compensated in the tuned basins (Fig. 2). In general, the differences between the six independent estimates of global long-term average water resources, which encompass a range between 36,000 and 44,000 km^3/yr, are much higher than the global consumptive water use.

While long-term averages of runoff and discharge are indicative of the spatially heterogeneous distribution of water resources, they cannot be regarded as exhaustive indicators for water availability. Interannual and seasonal variability needs to be taken into account to assess water stress that arises from a discrepancy between water demand and water availability. To show the impact of interannual variability on water availability, the runoff in the cell-specific 1-in-10 dry year is compared to the long-term average total cell runoff of the time period 1961–1990 (in 90%

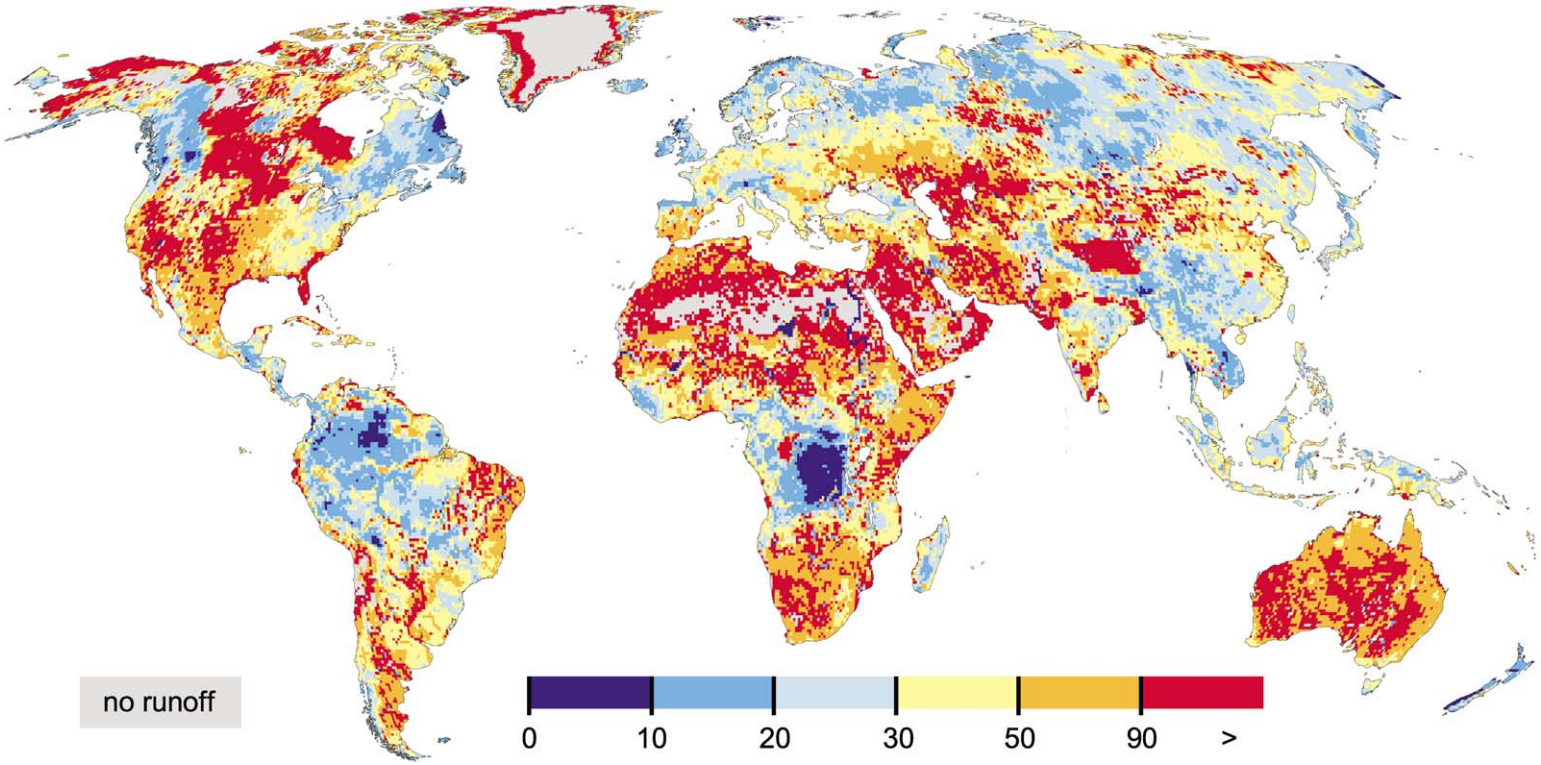

Fig. 6. Relative reduction of total runoff in 1-in-10 dry year as compared to the long-term average annual total runoff (time period 1961–1990), in %.

of the years, runoff is higher than in the 1-in-10 dry year). Fig. 6, together with Fig. 5, shows that interannual runoff variability is highest in those regions of the globe with a low average cell runoff. The 1-in-10 dry year runoff provides a stronger spatial discrimination of the water resources situation than the long-term average runoff and represents the situation in a potential crisis year; therefore, it is a useful additional indicator of water availability.

Whenever annual averages are considered in an assessment of water availability, it is implicitly assumed that storage capacities (e.g. in aquifers or man-made reservoirs) exist to make the total annual discharge available whenever it is needed. However, this is only the case in a few strongly developed drainage basins like the Egyptian Nile. In the other basins, the discharge during the periods of high flow can generally not be used to fulfill human water demand. Therefore, a water availability indicator which takes into account seasonal variability is needed. The 90% reliable monthly discharge Q_{90}, which is equal to the discharge that is exceeded in 9 out of 10 months, provides an estimate of the discharge that can be relied on for water supply. The Q_{90} derived from WGHM calculations takes into account any reduction of natural discharge by upstream consumptive water use. The global distribution of the 1961–1990 Q_{90} (Fig. 7) shows that discharge and thus water availability is concentrated along the major river courses, in particular in arid and semi-arid zones. The spatial heterogeneity of Q_{90} is higher than that of the long-term average discharges (not shown). A continental aggregation of the Q_{90} discharged into the oceans and inner-continental sinks is also provided in Table 1. It represents the annual renewable discharge that is available if it is assumed that the amount of water that can be used in each month of the year is equal to the Q_{90}-value. At the global scale, the thus computed water availability is only 32% of the long-term average water resources. The continent which shows the highest seasonal variability of discharges is Asia, where only 18% of long-term annual water resources is reliably available. South America is the continent with the lowest seasonal variability, and the Q_{90} water availability accounts for 41% of the total water resources.

5. Model performance

In this section, we discuss the ability of WGHM to compute the water availability indicators presented above. In Sections 5.1 and 5.2, the performance of WGHM at the tuning stations is shown, and in Section 5.3. the performance in other cells (validation stations).

5.1. Global analysis of tuning stations

WGHM is tuned such that the simulated long-term average discharge is within 1% of the observed value. However, the temporal dynamics of the model, i.e. the year-to-year or month-to-month variability of discharge, are not directly affected by the tuning process. Therefore, the comparison of simulated and observed annual and monthly discharge time series at the tuning stations can serve to test the model performance. The quality of simulating the interannual variability of discharge at the tuning points is measured by the modeling efficiency (Janssen and Heuberger, 1995) with respect to annual discharge values AME. The modeling efficiency, also known as Nash–Sutcliffe coefficient, relates the goodness-of-fit of the model to the variance of the measurement data and thus describes the modeling success with respect to the mean of the observations. Different from the correlation coefficient, it indicates a high model quality only if the long-term average discharge is captured well. If AME is larger than 0.5, the interannual variability of discharge is represented well by the computation.

Fig. 8 presents the AME of all 724 tuning basins and shows the capability of WGHM to simulate the sequence of wet and dry years. AME indicates how well runoff or discharge in the 1-in-10 dry year can be modeled. In most of Europe and the USA, AME is above 0.5, and for many basins, AME is even above 0.7. All the basins in China and most of the Siberian basins show an AME higher than 0.5, while the situation in mixed in the rest of Asia. The Ganges, the lower Indus, the Amu Darya and some smaller basins in Central India are modeled well with respect to their interannual variability, but other basins including the Brahmaputra, Irrawaddy, Syr Darya and most basins in the Near East are not. In the case of the Brahmaputra and Irrawady, this might be related to an inaccurate precipitation input (compare Section

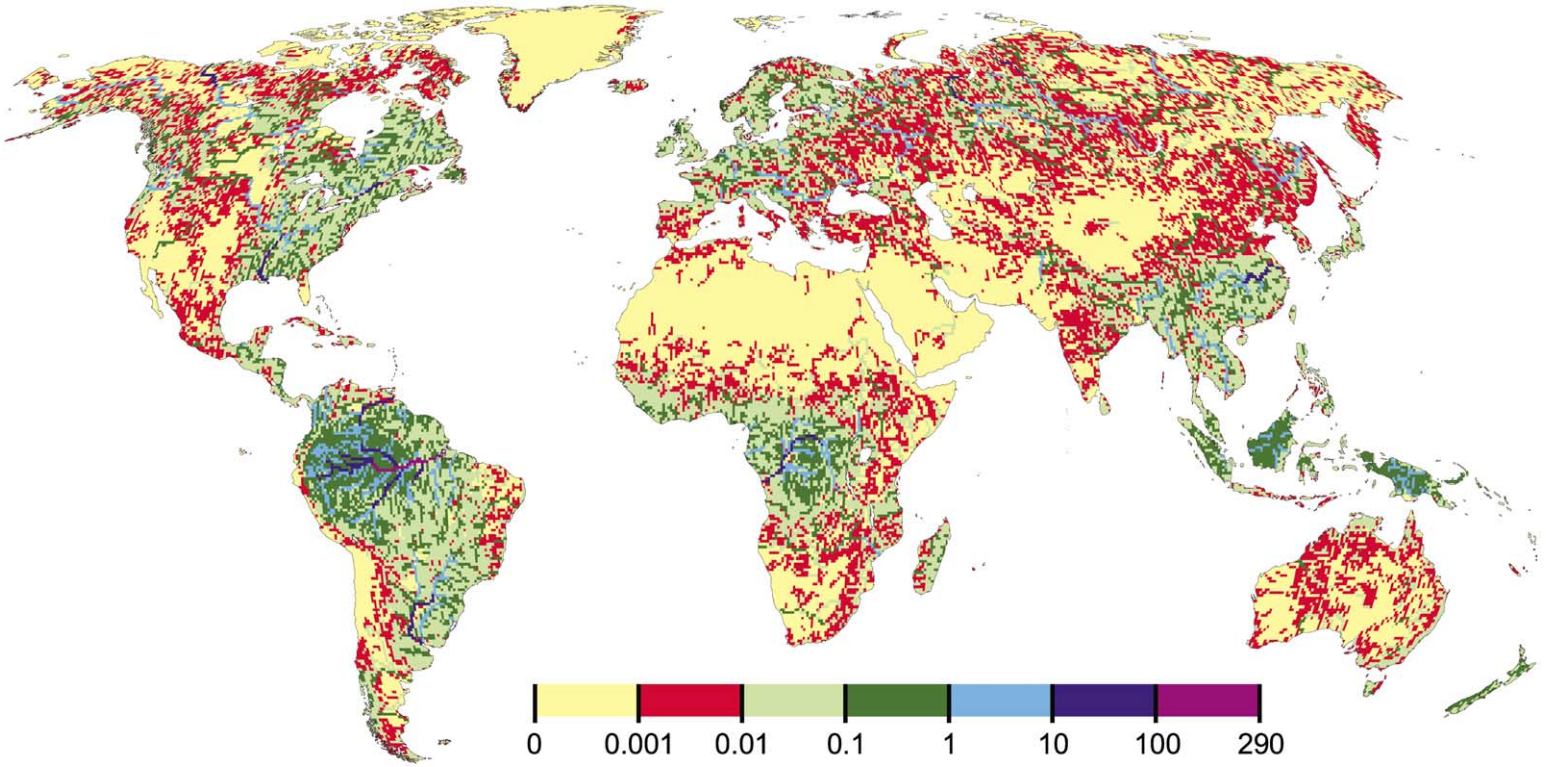

Fig. 7. 90% reliable monthly discharge Q_{90} (time period 1961–1990), in km^3/month.

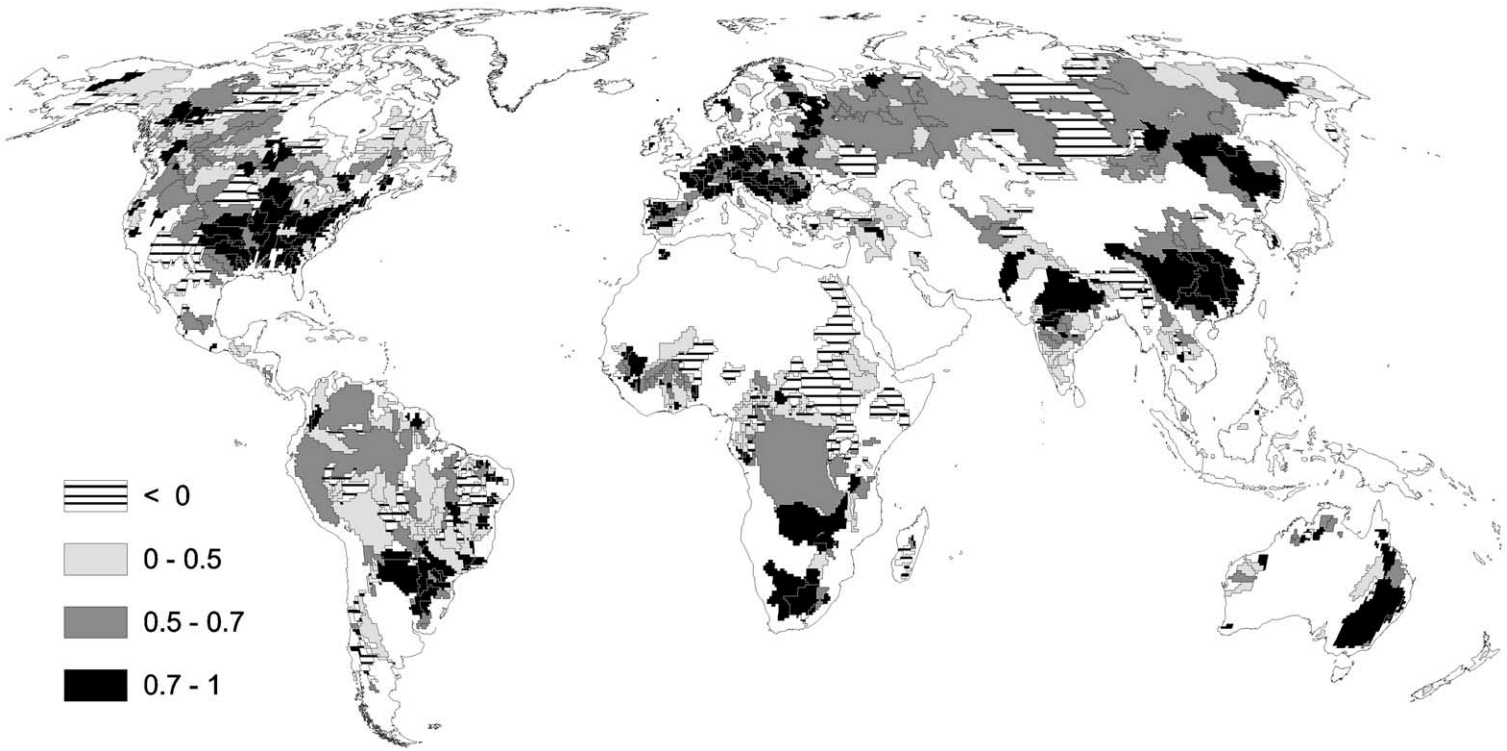

Fig. 8. Modeling efficiency of annual discharges at 724 tuning stations (for the respective tuning periods).

Table 2
Global summary of WGHM model performance with respect to the modeling efficiency of the annual river discharges AME and the 90% reliable monthly discharge Q_{90}, distinguishing three classes of tuning basins: humid basins, semi-arid and arid basins, and snow-dominated basins

	Humid[a]	Semi-arid and arid[b]	Snow-dominated[c]	Total
AME				
Total number of tuning basins	389	191	144	724
% of basins with AME $>$ 0.7	34	27	13	28
% of basins with 0.5 $<$ AME $\leq$ 0.7	20	26	31	24
Q_{90}				
Total number of tuning basins considered for Q_{90} comparison[d]	201	91	88	380
% of basins where difference between observed and simulated Q_{90} is smaller than 10% of the long-term average discharge	48	74	40	53
% of basins where difference between observed and simulated Q_{90} is 10–20% of the long-term average discharge	31	16	26	26
Average absolute difference between observed and simulated Q_{90} in % of long-term average discharge	12	10	17	13

[a] Basins in which long-term average (1961–1990) precipitation is more than 50% of long-term average potential evapotranspiration (but not snow-dominated)
[b] Basins in which long-term average (1961–1990) precipitation is less or equal 50% of long-term average potential evapotranspiration (but not snow-dominated)
[c] Basins where more than 30% of the precipitation falls as snow
[d] Basins with drainage areas greater han 20,000 km^2, and observed discharge series of at least 15 years

3.6). In Africa, most basins north of the equator do not perform well, while the interannual variability of the Central African Congo and the semi-arid to arid Southern African basins of the Zambezi and Orange is captured. Model performance on the American continent outside the USA is variable, and for most of the Australian basins it is satisfactory. In general, the likelihood of a good AME is higher for basins that do not require runoff correction (compare Fig. 3). However, even some of the other basins reach good AME, e.g. the lower Danube (Europe), the Yangtze (China), the Murray–Darling (Australia) and the Orange (South Africa) basins. Table 2 shows that snow-dominated basins (with more than 30% of the long-term average precipitation falling as snow) perform worse than the other basins. In the case of humid and semi-arid/arid basins that are not snow-dominated, 54 and 53%, respectively, of all tuning basins have an AME greater than 0.5, and 34% of the humid basins and 27% of the semi-arid/arid one have an AME that is even above 0.7, compared to only 13% of the snow-dominated basins

The modeling efficiency with respect to monthly discharge values MME takes into account the coincidence of simulated and observed discharge in each individual month. A rather small temporal lag between measured and observed peaks will lead to a negative MME (compare Section 5.2 below). For most tuning basins, MME is below 0.5; exceptions are, for example, the Ganges and Yangtze basins and basins in Siberia and Western Europe.

The capability of WGHM to simulate the 90% reliable monthly discharge Q_{90} is checked by comparing simulated Q_{90}-values to those derived from the time series of observed discharges. Unfortunately, the observed discharge time series are often too short to derive a reliable value of observed Q_{90}. For the comparison, only those 380 stations were selected which have been tuned for at least 15 complete measurement years and represent a drainage area of more than 20,000 km^2. Fig. 9 (left) shows the correspondence between simulated and observed Q_{90}. Obviously, the very high modeling efficiency of 0.98 is due to the good fit of the two largest values. For some basins, in particular the smaller ones, simulated and observed Q_{90} differ by a factor of 10, but for most basins, the difference is less than a factor of 2. While this check illustrates the capability of the model to derive realistic estimates of Q_{90} (in km^3/month), the quality of

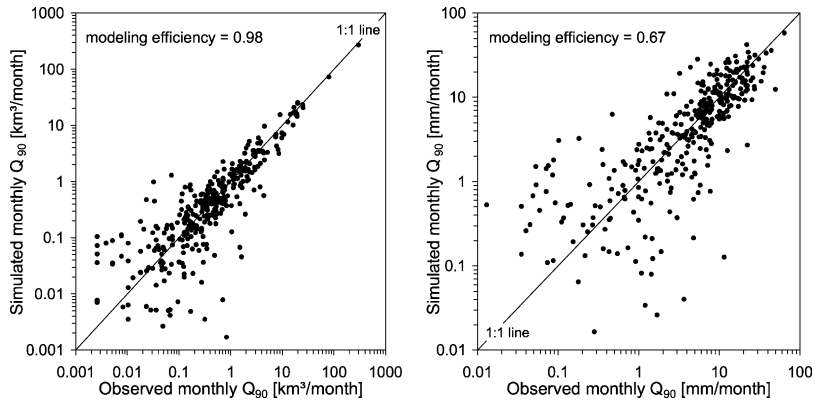

Fig. 9. Comparison of simulated and observed 90% monthly reliable discharge Q_{90} for the 380 tuning stations with a drainage area of more than 20,000 km^2 and an observed time series of at least 15 years (for the respective tuning periods). Left: Q_{90} in km^3/month, right: area-specific Q_{90} in mm/month.

the model with respect to the translation of precipitation into discharge is better judged by comparing the Q_{90} per unit drainage basin area (in mm/month). The area-specific Q_{90} filters out the impact of the drainage basin size. Modeling efficiency for the area-specific Q_{90} is reduced to 0.67 (Fig. 9 right). If only the 144 stations with discharge observations for the whole period of 1961–1990 are considered (hence the observed area-specific Q_{90} is more reliable), model efficiency increases to 0.73. Finally, it increases to 0.81 if from the previous selection only the 97 basins with an area of more than 50,000 km^2 are taken into account. For basins smaller than 20,000 km^2, the modeling efficiency is low. We conclude that the performance of WGHM with respect to simulating Q_{90} is satisfactory for basins with at least 20,000 km^2, and improves with increasing basin size.

Table 2 provides summary statistics of the model performance with respect to Q_{90}. In 79% of the 380 basins, the difference between simulated and observed Q_{90} is less than 20% of the long-term average discharge, and in 53%, it is even less than 10%. In semi-arid/arid basins, the average difference between simulated and observed is 10% of the long-term average discharge, while it is 13% and 17% in the case of humid and snow-dominated areas, respectively.

5.2. Selected tuning stations

To get a better impression of the quality of WGHM, its performance at eight selected stations with long time series of observed discharge is discussed in the following. Fig. 2 shows the location of these stations, and Table 3 lists observed and simulated discharge variables, long-term average discharge, 90% reliable monthly discharge Q_{90} and 10% reliable monthly discharge Q_{10}. Besides, it provides the modeling efficiencies for monthly (MME) and annual (AME) discharges as well as the basin area and the area-specific discharge. As an example, Fig. 10 shows the time series of annual (top) and monthly (bottom) discharges of the Polish Wisla river (at gauging station Tczew). With an AME of 0.65, the sequence of observed wet and dry years is captured well by the model, even though there is a slight overestimation of observed discharge in the 1960s and an underestimation in particular in 1980. The monthly time series has a MME of 0.54. The underestimation in the summer months is particularly high in the 1960s, while the high peak flows in the summer of 1980 are clearly missed by the model. In general, low flows of the Wisla are represented very well by WGHM, which is shown by the very good correspondence of simulated and observed Q_{90} (Table 3). The high flows as expressed by the monthly Q_{10} are somewhat lower than in reality. This can also be seen in Fig. 11, which shows the mean monthly hydrograph of the period 1961–1990. The underestimation of flow in January and February and the overestimation in March and April is rather typical for WGHM in the case of river basins with seasonal snow. This is due to the simple snow modeling

Table 3
Comparison of observed and simulated discharge at selected tuning stations: long-term average discharge, 90% reliable monthly discharge Q_{90} and 10% reliable monthly discharge Q_{10}. (Q_{spec}: observed specific discharge per unit area of drainage basin, MME: modeling efficiency for monthly discharge, AME: modeling efficiency for annual discharge)

	Area[a] (1000 km^2)	Runoff coeff. [b]	Period	Q_{spec} (mm/yr)	Long-term average discharge (km^3/month)		Monthly Q_{90} (km^3/month)		Monthly Q_{10} (km^3/month)		MME	AME
					obs.	sim.	obs.	sim.	obs.	sim.		
Wisla at Tczew, Poland	194	0.98	61–90	181	2.93	2.91	1.50	1.49	4.93	4.58	0.54	0.65
Danube at Achleiten, Germany	76	0.38	61–90	592	3.75	3.76	2.13	1.04	5.58	6.79	<0	0.80
Yenisei at Igarka, Russia	2456	0.3	61–90	231	47.38	48.20	13.26	10.10	91.49	86.13	0.85	<0
		$f_c = 1.60$										
Mekong at Chiang Saen, Thailand	195	0.30	61–90	439	7.14	7.11	2.20	1.08	15.25	16.84	0.74	0.54
Guadalquivir at Alcalá del Río, Spain	46	0.67	61–90	86	0.33	0.31	0.05	0.00	0.80	0.87	0.42	0.50
Senegal at Kayes, Mali	159	3	61–90	81	1.07	1.06	0.01	0.11	3.29	2.77	0.82	0.73
		$f_c = 0.59$										
		$f_s = 0.94$										
Waterhen at Waterhen, Canada	59	0.52	61–88	39	0.19	0.18	0.02	0.14	0.38	0.24	0.17	0.35
Gascoyne at Nune Mile Bridge, Australia	78	2.70	61–90	8	0.05	0.05	0.00	0.00	0.09	0.15	0.33	0.46

[a] According to DDM30 drainage direction map used in WaterGAP 2.
[b] f_c: runoff correction factor, f_s: discharge correction factor (at station).

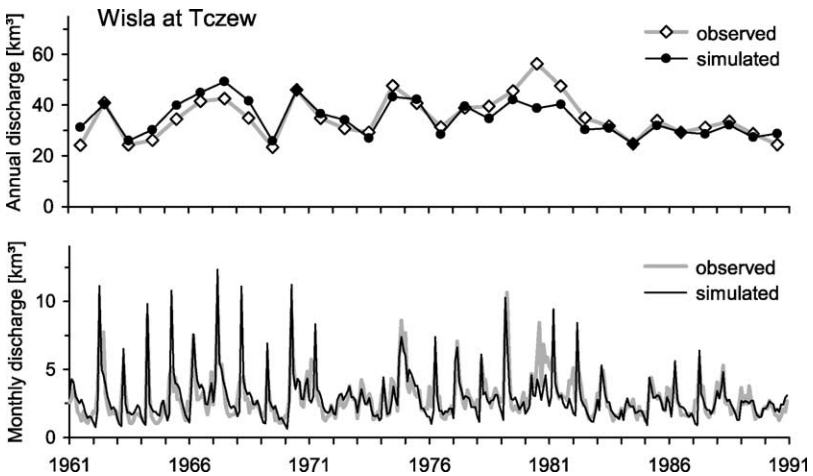

Fig. 10. Comparison of simulated and observed discharge of the Wisla river at Tczew (tuning station): time series of annual discharge (top), time series of monthly discharge (bottom).

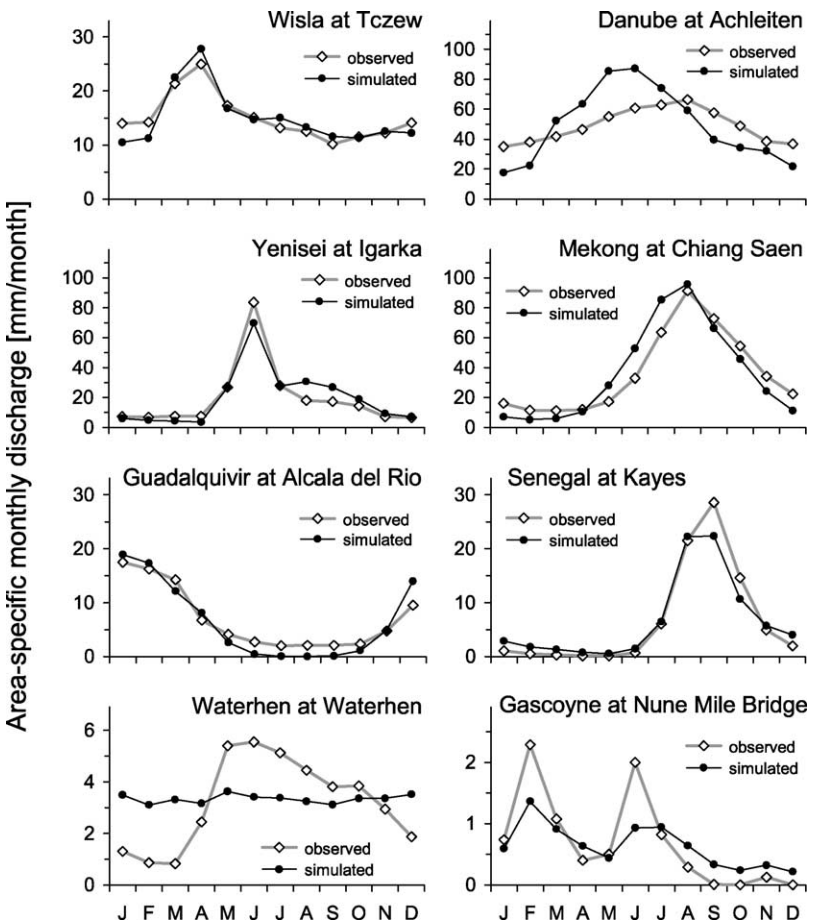

Fig. 11. Comparison of simulated and observed mean monthly hydrographs at eight selected tuning stations (compare Table 3).

approach of WGHM, with interpolated monthly temperatures and a homogeneous temperature throughout each grid cell. In the model, too much precipitation is stored as snow until the end of the winter, which leads to an underestimation of discharge during winter and an overestimation during spring. In reality, even in months with an average temperature below 0 °C there are days or at least hours above 0 °C, and due to the different microclimates within a grid cell, not everywhere in the cell average temperature is below 0 °C. Hence, snowfall and snowmelt occur in a spatially and temporally more heterogeneous way than simulated by WGHM.

The mean monthly hydrograph of the Danube at Achleiten (Fig. 11) shows another example for the effect of the coarse treatment of snow in the model. Additionally, the observed peak discharge in September is strongly influenced by Alpine tributaries with glacier melting (not captured in WGHM), and the reduced seasonal variability of the observed discharge is caused by the management of reservoirs in the tributaries of the Danube (unknown in WGHM). Although the seasonal behavior is not simulated satisfactorily, the interannual variability is represented well (AME = 0.80). The Yenisei at Igarka, which requires a runoff correction probably due to the precipitation measurement bias, is an example for the opposite behavior. The seasonal regime being captured very well even though the basin is snow-dominated and permafrost and freezing of the soil is not considered in the model. The interannual variability, however, is not correctly simulated. The Mekong at Chiang Saen is also influenced by snow, and at least part of the overestimated seasonal variability of flows might by due to the coarse snow modeling.

While the above basins are in humid regions and have area-specific discharges between 180 and 600 mm/yr (Table 3), the next four basins shown in Fig. 11 are in semi-arid and arid regions and have area-specific discharges between 8 and 86 mm/yr. For both the Guadalquivir and the Senegal, the seasonal regime and the interannual variability are captured quite well, even though in the (highly developed) Guadalquivir basin, the simulated discharge drops to zero in the summer, which is not the case in reality. For the Senegal at Kayes, both the runoff of the basin and the discharge at the station had to be corrected, and the good correspondence of simulated and observed discharge indicates that the channel and other evaporation losses that are not simulated explicitly by the model are proportional to the discharge. The gauging station at the Waterhen in Canada is located between two lakes, and the simulation of lake storage leads to a discharge that is almost constant throughout the year, while the observed discharge shows a rather high seasonality. This indicates that the simulation of lake storage in WGHM is not adequate. The very low discharges of the Western Australian river Gascoyne are not represented well even though the long-term average discharge can be modeled without any runoff or discharge correction.

5.3. Selected validation stations

An important test of the quality of the WGHM is to check how well simulated discharge fits to observed discharge at gauging stations that were not used for tuning. Like Table 3 for selected tuning stations, Table 4 lists observed and simulated discharge variables as well as modeling efficiencies for nine validation stations (located in Fig. 2). Six of these stations are located within drainage basins that were tuned, none of them being downstream of a tuning station. The other three are outside tuning basins, and their runoff coefficients have been determined by regionalization.

The most important discharge variable to be compared is the long-term average discharge. For the example of the Saale at Calbe, which is located within the tuned Elbe basin (132,510 km^2 at the tuning station Neu-Darchau), the simulated long-term average discharge is only 6% higher than the observed value. Fig. 12 shows the time series of annual (top) and monthly (bottom) discharges of the Saale at Calbe. The interannual variability is captured quite well (AME = 0.65), while the monthly discharges show a rather low correspondence (MME = 0.31). Before 1988, the WGHM often simulates a very low discharge in January, probably due to freezing conditions. After 1991, the summer low flows were not captured well anymore, which might be due to neglecting capillary rise from the groundwater, a process which possibly became important due to decreased drainage of lowlands after the reunification

Table 4
Comparison of observed and simulated discharge at selected gauging stations that have not been used for model tuning (validation stations): long-term average discharge, 90% reliable monthly discharge Q_{90} and 10% reliable monthly discharge Q_{10}

*	Area[a] (1000 km^2)	Runoff coeff.[b]	Period	Q_{spec} (mm/yr)	Long-term average discharge (km^3/month)		Monthly Q_{90} (km^3/month)		Monthly Q_{10} (km^3/month)		MME	AME
					obs.	Sim.	obs.	sim.	obs.	sim.		
Saale at Calbe, Germany	23	0.76 c	81–95	167	0.32	0.34	0.16	0.17	0.53	0.55	0.31	0.65
Maas at Borgharen, Belgium	22	3 c $f_c = 0.90$	61–90	338	0.62	0.70	0.09	0.15	1.47	1.49	0.75	0.82
Mamoré at Guajará–Mirim, Brazil[c]	614	0.59 c	71–90	438	22.39	22.51	5.23	6.11	41.48	45.02	<0	<0
						22.44		*8.31*		*41.10*	*0.78*	*0.40*
Içа at Ipiranga Velho, Brazil	108	0.3 c $f_c = 1.28$	80–90	2098	18.88	18.11	11.41	13.29	26.30	23.66	0.17	<0
Zambezi at Katima Mulilo, Namibia[d]	329	2.26 c	65–89	126	3.46	2.21	0.84	0.09	8.39	6.74	0.15	<0
		1.60				*3.25*		*0.24*		*8.39*	*0.80*	*0.74*
Cimarron at Perkins, OK, USA	45	2.76 c	61–87	27	0.10	0.12	0.01	0.02	0.24	0.29	0.35	0.40
Cunene at Ruacana, Namibia	89	1.60 r	62–78	61	0.45	0.74	0.08	0.10	1.02	1.90	<0	<0
Okavango at Rundu, Namibia	54	2.14 r	61–89	107	0.48	0.54	0.11	0.10	1.13	1.03	0.31	<0
Tombigbee at Coatopa AL, USA	44	1.19 r	61–87	513	1.88	1.97	0.27	0.60	4.99	4.33	0.83	0.90

(Q_{spec}: observed specific discharge per unit area of drainage basin, MME: modeling efficiency for monthly discharge, AME: modeling efficiency for annual discharge). *data sources: Saale: Potsdam Institute for Climate Impact Research, Potsdam, Germany; Maas: GRDC, Brazilian rivers: Center for Sustainability and the Global Environment (SAGE), University of Wisconsin—Madison; rivers in USA: HCDN Streamflow Data Set, 1874–1988 by J.R. Slack, Alan M. Lumb, and Jurate Maciunas Landwehr, USGS Water-Resources Investigations Report 93-4076; rivers in Namibia: Department of Water Affairs, Windhoek, Namibia.

[a] According to DDM30 drainage direction map used in WaterGAP 2.

[b] c: Station in basin for which runoff coefficient was tuned against discharge at a downstream station, without tuning upstream; r: station within basin for which runoff coefficient was determined by regionalization; f_c: runoff correction factor.

[c] In italics: results with a river transport velocity of 0.1 m/s instead of the standard value of 1 m/s.

[d] In italics: results with a runoff coefficient of 1.6 and river transport velocity of 0.18 m/s.

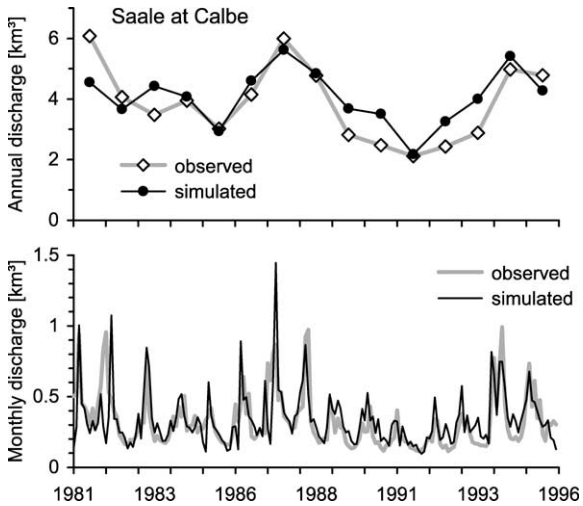

Fig. 12. Comparison of simulated and observed discharge of the Saale river at Calbe (validation station): time series of annual discharge (top), time series of monthly discharge (bottom).

of Germany. The mean monthly hydrograph (Fig. 13) again shows the effect of the coarse snow modeling, with a sudden discharge increase in March. Nevertheless, the Q_{90}- and Q_{10}-values are simulated very well (Table 4).

The Maas at Borgharen also shows a very good fit even though the station is located within a tuning basin that required runoff correction (Table 4, not shown in Fig. 13). The simulated and observed long-term average discharges of the Mamoré in the Amazon basin only differ by less than 1%, and the Q_{90}- and Q_{10}-values are simulated well. However, the simulated peak flows generally occur three to five months too early (Fig. 13, 'simulated A'). In the Amazon basin, large areas are seasonally flooded, which leads to a strong delay of peak flows. If discharge is simulated with a lower river flow velocity of 0.1 m/s instead of the rather high standard value of 1 m/s (compare Table 1 of Oki et al., 1999), the mean monthly hydrograph fits well (Fig. 13, 'simulated B') and the modeling efficiencies increase from below zero to 0.78, for MME, and 0.40, for AME. Another sub-basin of the Amazon basin, the Içа at Ipiranga Velho has a very high area-specific discharge of 2100 mm/yr and is located in a tuning basin which required a runoff correction (Table 4, not shown in Fig. 13). Nevertheless, the observed and simulated long-term average discharges as well as the Q_{90}- and Q_{10}-values fit well. The low modeling efficiency is, as

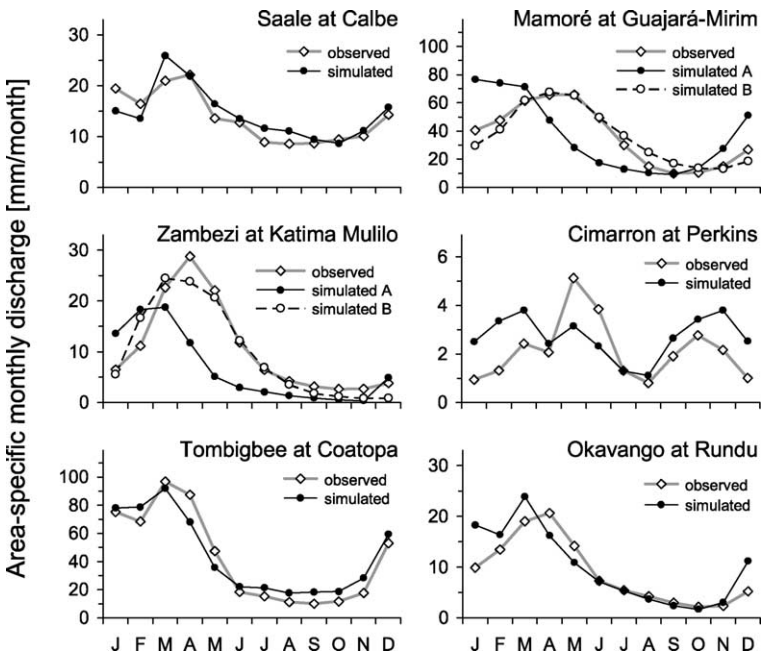

Fig. 13. Comparison of simulated and observed mean monthly hydrographs at six selected validation stations (compare Table 4).

in the case of the Mamoré, due to overestimation of lateral transport velocity.

The Zambezi at Katima Mulilo is within the tuning basin of the Zambezi at Matundo Cais, with a drainage area of more than 1.1 million km^2. Discharge at Matundo Cais is best simulated with a runoff coefficient of 2.26, which, however, leads to a significant discharge underestimation of 36% at Katima Mulilo (Fig. 13, simulated A). Obviously, the runoff generation within the large and heterogeneous drainage basin of the Zambezi cannot be captured by assigning one homogeneous runoff coefficient to the whole basin. The value of tuning for this station is shown by adjusting both the runoff coefficient and the lateral transport velocity. With a runoff coefficient of 1.60 and a lateral transport velocity of 0.18 m/s instead of 1 m/s, the long-term average discharge is underestimated by only 6%, and the modeling efficiencies increase to 0.80 (MME) and 0.74 (AME) (Table 4 and Fig. 13, simulated B). The Cimarron drains a rather dry region of the Arkansas basin. WGHM overestimates long-term average discharge by 20% and does not represent the seasonal regime (Fig. 13). Still, the Q_{90}- and Q_{10}-values are simulated quite well.

In summary, the quality of the simulated discharge at cells inside tuned basins appears to be reasonably good if the basin is rather homogeneous. The simulated long-term average discharges at the stations inside the relatively homogeneous Central European and Amazon basins fit well to the observed values, which is not the case for the more heterogeneous basins of the Zambezi and the tributaries of the Mississippi.

Finally, the model results at three gauging stations that are located outside of tuning basins (Fig. 2) are checked against observations (Table 4). The long-term average discharge in the dry Cunene basin (not shown in Fig. 13) is overestimated by more than 60%. This might be due to the rather low regionalized value of the runoff coefficient of 1.60 (even though this is the value that leads to a good fit for the nearby Zambezi at Katima Mulilo). Long-term average discharge in the somewhat wetter Okavango basin is overestimated by 13%, but the simulated Q_{90}- and Q_{10}-values fit the observed values well. The low flow period is particularly well captured (Fig. 13). However, the interannual variability is not reflected at all by the model. The Tombigbee in the humid Southeast of the USA is simulated very well by WGHM (Fig. 13). The long-term average discharge is overestimated by less than 5%, and the modeling efficiencies are high (AME = 0.90, MME = 0.83).

6. Conclusions

1901–1995 time-series of 0.5 degree gridded monthly runoff and river discharge are computed by a tuned version of the Global Hydrological Model of WaterGAP 2 (WGHM). Based on these time series, a number of relevant indicators of water availability can be computed in a consistent manner for the whole global land area (with the exception of Antarctica). They include 1) the long-term average annual renewable water resources, 2) the discharge or runoff in a typical dry year, e.g. in the 1-in-10 dry year, and 3) the 90% reliable monthly discharge Q_{90}. The latter two indicators take into account the impact of interannual and seasonal variability on water availability. On the global average, the 90% reliable water availability is computed to be only about one third of the long-term average water resources.

WGHM shows the following characteristics:

- It is based on the best global data sets that are currently available (in particular climate, drainage directions and wetlands, lakes and reservoirs).
- Due to model tuning and, if necessary, runoff and discharge correction, WHGM computes discharge at more than 700 gauging stations (representing about 50% of the global land area and 70% of the actively discharging area) such that the simulated long-term average discharge is within 1% of the observed value.
- The reduction of river flow by human water consumption is simulated based on results from the Global Water Use Model of WaterGAP 2.
- The impact of climate variability on water availability is taken into account. This includes the simulation of the impact of climate variability on upstream irrigation water requirements.
- Due to the coupling with the Global Water Use Model, WGHM can be used to estimate the impact of upstream water use changes on downstream water availability.

The quality of WGHM and its capability to simulate the above water availability indicators was tested by comparing observed and simulated discharge at the 724 tuning stations and also at nine other selected gauging stations. In general, the performance of the model with respect to computing the interannual variability as well as the 90% monthly reliable discharge increases with increasing basin size. We conclude that reliable results can be obtained for basins of more than 20,000 km^2.

However, basin types have been identified that are less likely to be represented well by WGHM. There is the tendency that semi-arid and arid basins are modeled less satisfactorily than humid basins, which is partially due to neglecting river channel losses and evaporation of runoff from small ephemeral ponds in the model. Also, the hydrology of highly developed basins with large artificial storages, basin transfers and irrigation schemes cannot be simulated well. In all basins where discharge is controlled by man-made reservoirs, its seasonality is likely to be misrepresented by WGHM as no information on reservoir management is taken into account. Snow-dominated river basins generally suffer from the underestimation of actual precipitation. Hence, in snow-dominated basins without a tuning station, discharge is likely to be underestimated. The seasonality of discharge in snow-dominated basins is not represented well by WGHM due to the simple snow-modeling algorithm used. River basins which are characterized by extensive wetlands and lakes are also difficult to model. Even though the explicit modeling of wetlands and lakes leads to a much improved modeling of both the vertical water balance and the lateral transport of water, not enough information is included in WGHM to accurately capture the hydrology of these water bodies.

We conclude that model tuning which aimed at achieving a good representation of the long-term average discharges has a strong positive effect on the performance of all proposed water availability indicators. Certainly, the reliability of model results is highest at the locations at which WGHM was tuned. It can be assumed that also the reliability for cells inside tuned basins is reasonably high if the basin is relatively homogeneous. This assumption is supported by the comparison of observed and simulated discharge at the gauging stations that were not used for tuning. No conclusion can be drawn with respect to the reliability of model results outside tuned basins but the discharge analysis at the few available stations indicates an acceptable reliability, in particular in humid regions.

Future model improvements will focus on a more realistic snow modeling, a refined modeling of groundwater recharge and the simulation of river channel losses. Besides, it is planned to include river velocity as an additional tuning parameter.

It has been shown that WGHM is able to compute reliable and meaningful indicators of water availability at a high spatial resolution. Therefore, the modeling results of WGHM are well suited to be used in global assessments of water security, food security and freshwater ecosystems.

Acknowledgements

The authors thank B. Fekete and an anonymous reviewer for their detailed and constructive comments.

References

Alcamo, J., Leemans, R., Kreileman, E. (Eds.), 1998. Global Change Scenarios of the 21st Century. Results of the IMAGE 2.1 Model, Pergamon, Oxford.

Alcamo, J., Henrichs, T., Rösch, T., 2000. World Water in 2025—Global modeling and scenario analysis for the World Commission on Water for the 21st Century, Kassel World Water Series 2, Center for Environmental Systems Research, University of Kassel, Germany, http://www.usf.uni-kassel.de/usf/archiv/dokumente.en.htm.

Arnell, N.W., 1999a. A simple water balance model for the simulation of streamflow over a large geographic domain. J. Hydrol. 217, 314–335.

Arnell, N.W., 1999b. Climate change and global water resources. Global Environ. Change 9, S31–S49.

Batjes, N.H., 1996. Development of a world data set of soil water retention properties using pedotransfer rules. Geoderma 71, 31–52.

Baumgartner, A., Reichel, E., 1975. The World Water Balance, Elsevier, Amsterdam.

Bergström, S., 1995. The HBV model. In: Singh, V.P., (Ed.), Computer Models of Watershed Hydrology, Water Resources Publications, pp. 443–476.

Birkett, C.M., Mason, I.M., 1995. A new global lakes database for a remote sensing programme studying climatically sensitive large lakes. J. Great Lakes Res. 21 (3), 307–318.publication available online at http://wwwcpg.mssl.ucl.ac.uk/orgs/un/glaccd/html/mgld.html.

Brown, J., Ferrians, O.J. Jr., Heginbottom, J.A., Melnikov, E.S., 1998. Digital Circum-Arctic Map of Permafrost and Ground-Ice Conditions. International Permafrost Association Data and Information Working Group, Circumpolar Active-Layer Permafrost System (CAPS), CD-ROM version 1.0. National Snow and Ice Data Center, University of Colorado, Boulder, Colorado.

Canadian Geological Survey, 1995. Generalized Geological Map of the World and Linked Databases. Open File Report 2915d. CD-ROM.

Deardorff, J.W., 1978. Efficient prediction of ground surface temperature and moisture, with inclusion of a layer of vegetation. J. Geophys. Res. 86C, 1889–1903.

Döll, P., Lehner, B., 2002. Validation of a new global 30-min drainage direction map. J. Hydrol. 258 (1–4), 214–231.

Döll, P., Siebert, S., 2002. Global modeling of irrigation water requirements. Water Resour. Res. 38 (4), 8.1–8.10.DOI 10.1029/2001WR000355.

Döll, P., Kaspar, F., Lehner, B., 2001. The global integrated water model WaterGAP 2.1. In: Lehner, B., Henrichs, T., Döll, P., Alcamo, J. (Eds.), EuroWasser, Kassel World Water Series 5, Center for Environmental Systems Research, University of Kassel, Germany, http://www.usf.uni-kassel.de/usf/archiv/dokumente.en.htm.

Döll, P., Lehner, B., Kaspar, F., 2000. Global modeling of groundwater recharge and surface runoff. EcoRegio 8, 73–80.

Döll, P., Kaspar, F., Alcamo, J., 1999. Computation of global water availability and water use at the scale of large drainage basins. Mathematische Geologie 4, 111–118.

ESRI (Environmental Systems Research Institute), 1992. ArcWorld 1:3 M Continental Coverage.

ESRI (Environmental Systems Research Institute), 1993. Digital Chart of the World 1:1 M.

FAO (Food and Agriculture Organization), 1995. Digital Soil Map of the World and Derived Soil Properties, CD-ROM Version 3.5, FAO, Rome.

Fekete, B.M., Vörösmarty, C.J., Grabs, W., 1999. Global composite runoff fields of observed river discharge and simulated water balances. Report No. 22, Global Runoff Data Centre, Koblenz, Germany.

Forsythe, W.C., Rykiel, E.J., Stahl, R.S., Wu, H., Schoolfield, R.M., 1995. A model comparison for daylength as a function of latitude and day of year. Ecol. Model. 80, 87–95.

Geng, S., Penning, F.W.T., Supit, I., 1986. A simple method for generating daily rainfall data. Agric. For. Meteor. 36, 363–376.

GRDC (Global Runoff Data Centre), 1999. GRDC Station Catalog (available online athttp://www.bafg.de/html/internat/grdc/download.html).

Hölzle, M., Häberli, W., 1999. World Glacier Inventory. World Glacier Monitoring Service. National Snow and Ice Data Center. University of Colorado, Boulder, Colorado.

ICOLD (International Commission on Large Dams), 1998. Word Register of Dams (CD-ROM), Paris, France.

Janssen, P.H.M., Heuberger, P.S.C., 1995. Calibration of process-oriented models. Ecol. Model. 83, 55–66.

Kaspar, F., Döll, P., Lehner, B., 2001. Globale Modellierung der Durchflussverminderung durch konsumptive Wassernutzung. In: Sutmöller, J., Raschke, E. (Eds.), Modellierung in meso-bis makroskaligen Flußeinzugsgebieten-Tagungsband zum gleichnamigen Workshop am 16./17. November 2000 in Lauenburg, GKSS 2001/15, GKSS Geesthacht,.

Klepper, O., van Drecht, G., 1998. WARibaS, Water Assessment on a River Basin Scale; A computer program for calculating water demand and satisfaction on a catchment basin level for global-scale analysis of water stress. Report 402001009. RIVM, The Netherlands.

Korzun, V.I., Sokolow, A.A., Budyko, M.I., Voskresensky, K.P., Kalininin, G.P., Konoplyanstev, A.A., Korotkevich, E.S., Kuzin, P.S., Lvovich, M.I. (Eds.), 1978. World Water Balance and Water Resources of the Earth. UNESCO, Paris,.

Legates, D.R., Willmott, C.J., 1990. Mean seasonal and spatial variability in gauge-corrected, global precipitation. Int. J. Climatotol. 10, 111–117.

Lehner, B., Döll, P., 2001. A global lakes, reservoirs and wetlands data set. Data set description sheet, Center for Environmental Systems Research, University of Kassel, Germany.

Liang, X., Lettenmaier, D.P., Wood, E.F., Burges, S.J., 1994. A simple hydrologically based model of land surface water and energy fluxes for general circulation models. J. Geophys. Res. D3 (99), 14415–14428.

Meigh, J.R., McKenzie, A.A., Sene, K.J., 1999. A grid-based approach to water scarcity estimates for Eastern and Southern Africa. Water Resour. Mgmt 13 (2), 85–115.

New, M., Hulme, M., Jones, P.D., 2000. Representing twentieth century space-time climate variability Part II: Development of 1901-96 monthly grids of terrestrial surface climate. J. Climate 13, 2217–2238.

Nijssen, B., O'Donnell, G.M., Lettenmaier, D.P., Lohmann, D., Wood, E.F., 2001. Predicting the discharge of global rivers. J. Climate 14, 3307–3323.

Oki, T., Nishimura, T., Dirmeyer, P., 1999. Assessment of annual runoff from land surface models using Total Runoff Integrating Pathways (TRIP). J. Meteorol. Soc. Jpn 77, 235–255.

Priestley, C., Taylor, R., 1972. On the assessment of surface heat flux and evaporation using large scale parameters. Mon. Weather Rev. 100, 81–92.

Raskin, P., Gleick, P., Kirshen, P., Pontius, G., Strzepek, K., 1997. Water futures: Assessment of long-range patterns and problems. Background paper Comprehensive Assessment of the Freshwater Resources of the World, Stockholm Environment Institute, Stockholm, Sweden.

Shuttleworth, W.J., 1993. Evaporation. In: Maidment, D.R., (Ed.), Handbook of Hydrology, McGraw-Hill, New York, USA, pp. 4.1–4.53.

Smedena, L., 2000. Irrigation-induced river salinization: Five major irrigated basins in the arid zone. International Water Management Institute, Colombo, Sri Lanka.

Vörösmarty, C.J., Federer, C.A., Schloss, A., 1998. Potential evaporation functions compared on US watersheds: implications for global-scale water balance and terrestrial ecosystem modelling. J. Hydrol. 207, 147–169.

Vörösmarty, C.J., Sharma, K., Fekete, B., Copeland, A.H., Holden, J., Marble, J., Lough, J.A., 1997. The storage and aging of continental runoff in large reservoir systems of the world. Ambio 26, 210–219.

WCMC (World Conservation Monitoring Centre), 1999. Wetlands Dataset, Cambridge, UK.

WRI (World Resources Institute), 2000. World Resources 2000–2001, Oxford University Press, New York, USA.

Yates, D.N., 1997. Approaches to continental scale runoff for integrated assessment models. J. Hydrol. 291, 289–310.